Advances in Water Resources 162 (2022) 104148

Contents lists available at ScienceDirect

Advances in Water Resources

journal homepage: www.elsevier.com/locate/advwatres

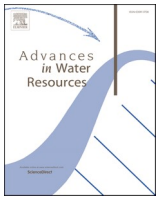

Wave attenuation by flexible vegetation (and suspended kelp) with blade motion: Analytical solutions

Longhuan Zhu [a,*], Kimberly Huguenard [a], David W. Fredriksson [b], Jiarui Lei [c]

[a] Department of Civil and Environmental Engineering, University of Maine, Orono, ME, USA
[b] Department of Naval Architecture and Ocean Engineering, U.S. Naval Academy, Annapolis, MD, USA
[c] College of Design and Engineering, National University of Singapore, Singapore

ARTICLE INFO

Keywords:
Wave attenuation
Vegetation
Kelp
Bulk drag coefficient
Effective blade length
Seasonal impacts

ABSTRACT

Vegetation is one of the most important components of nature-based coastal protection due to its ability to dissipate wave energy. To quantify the wave attenuation by vegetation, traditional analytical models assume rigid vegetation and use bulk drag coefficient (C_D) or effective blade length (l_e) techniques to consider the effects of blade motion, where C_D and l_e are conventionally fitted as a function of KC (the Keulegan–Carpenter number) and CaL (with Ca the Cauchy number and L the ratio of the blade length to wave excursion), respectively. These parameters do not include the full blade dynamics and so the empirical formulas of C_D and l_e are different for varying vegetation with blade dynamics. To obtain analytical solutions for C_D and l_e, an analytical wave attenuation model for flexible vegetation (and kelp) was developed in this study by simplifying and linearizing the blade motion. Compared with a wide range of experiments for both submerged vegetation and suspended kelp canopies, the simplified analytical model underestimated the wave decay coefficient (k_D) by 27%, but with a small NRMSE (normalized root mean square error by the range of the measured data) of 0.054. In comparison, the numerical model with full nonlinearity underestimated the wave decay coefficient by 11.7% with NRMSE=0.063. To reduce the underestimation of the analytical model due to the simplification and linearization, a modification factor defined as the ratio of the numerically calculated k_D and the analytically calculated k_D was fitted. With the modification factor, the underestimation of the analytical model was reduced to 10.1%. Based on the analytical model, analytical solutions for C_D and l_e were derived, which showed a similar precision with the experimentally fitted C_D and l_e based on KC and CaL, respectively. Thus, the analytical solutions for C_D and l_e could be a reliable alternative when the experimentally calibrated C_D and l_e are not available. Using the analytical wave attenuation model, a case study showed the wave attenuation by cultivated *Saccharina latissima* changes seasonally with the kelp growth. When the kelp blade reaches 2.4 m long after 7 months of growth, the kelp farms with 50 longlines (over a distance of 200 m in the direction of wave propagation) in 8 m-deep water may attenuate wave energy by 29% for 1 m-high waves with the period of 6 s. The wave attenuation can be enhanced to 43% when the farms are located in 5 m-deep water. To provide considerable wave attenuation of kelp with adequate long blades around the year, biennial and multiple partial harvesting techniques are recommended.

1. Introduction

Coastal communities are exposed to the increasing risks of coastal erosion and flooding from storm tides and rising sea levels (Izaguirre et al., 2011; Tebaldi et al., 2012; Ondiviela et al., 2014; Weinkle et al., 2018). Conventional hard structures are recognized to have adverse impacts on the environment and are less sustainable in a changing climate (Syvitski et al., 2009; Currin et al., 2010; Pace, 2011; Temmerman et al., 2013; Sutton-Grier et al., 2015). There is a growing need to use nature-based infrastructures for coastal defense (Morris et al., 2019; Möller, 2019; Zhu et al., 2020a). Nature-based infrastructures include wetland plants, mangroves, aquatic vegetation, kelp beds, coral reefs, and shellfish reefs. Based on the vertical position of the biomaterial in the water column, nature-based infrastructures are classified as either submerged (e.g., submerged aquatic vegetation located at the seafloor), emerged (e.g., saltmarsh and mangroves located

* Corresponding author.
E-mail address: longhuan.zhu@maine.edu (L. Zhu).

https://doi.org/10.1016/j.advwatres.2022.104148
Received 19 November 2020; Received in revised form 26 January 2022; Accepted 2 February 2022
Available online 3 February 2022

at the seafloor and emerged out of the water surface), suspended (e.g., kelp and mussel aquacultures suspended in the water column with gaps below and above the canopy), or floating (e.g., floating wetland) canopies. These canopies have the potential to protect coastal regions by damping wave energy without the adverse effects of hardened shorelines.

The wave attenuation by canopies has been investigated with laboratory and field experimental techniques as well as analytical and numerical models. Many of these methods are based on the wave attenuation theories developed by Dalrymple et al. (1984) and Kobayashi et al. (1993), assuming a rigid canopy component (referred to as 'blade' herein and after) without motion. Wave dissipation is dependent on the work of the canopy drag and therefore is proportional to the cube of the relative velocity between the flow and the blade. Neglecting the blade motion can overestimate wave attenuation. In an effort to represent these uncertainties, a bulk drag coefficient (C_D) approach has been applied (e.g., Kobayashi et al., 1993; Mendez and Losada, 2004). Alternatively, Luhar and Nepf (2016) and Luhar et al. (2017) proposed a technique that considers the effects of blade motion by using a reduced effective blade length (l_e) rather than the bulk drag coefficient (C_D) that reduces the original drag coefficient (C_d) for a rigid blade. The effective blade length (l_e) is defined as the length of a rigid blade that dissipates the same wave energy as the flexible blade with the original length (l). The bulk drag coefficient and effective blade length methods reduce the complexity of modeling the wave-vegetation interaction so that these models are computationally efficient and convenient to implement in large-scale models. However, numerous experiments are required to calibrate C_D and l_e. Conventionally, C_D is expressed as a function of the Reynolds number (Re) or Keulegan–Carpenter number (KC) independent from vegetation flexural rigidity. Thus, the Re- and KC-based empirical formulas for C_D are different for vegetation with different flexibilities, e.g., the different formulas in Mendez and Losada (2004), Bradley and Houser (2009), Sánchez-González et al. (2011), Jadhav et al. (2013), Anderson and Smith (2014), and Ozeren et al. (2014) as summarized in Chen et al. (2018) and van Veelen et al. (2020). The empirical formula for l_e is expressed as a function of the Cauchy number (Ca) incorporating vegetation flexural rigidity. Accurate parameterizations of C_D and l_e are important to predict wave attenuation (Fringer et al., 2019), which requires a full understanding of wave-vegetation interaction.

To quantify the blade motion in waves, the flexible blade is modeled as a cantilever beam using the Euler-Bernoulli beam approach. By simplifying the blade motion to a balance of drag force and blade bending resistance, Mullarney and Henderson (2010) obtained linear normal mode solutions for the blade displacement along the length of the blade. The model was recently extended to include the effects of buoyancy by Henderson (2019). With the normal mode technique, Zhu et al. (2020a) obtained frequency-dependent analytical solutions for blade displacements in random waves considering the effects of inertial forces. As the analytical solutions are limited to small-amplitude blade motion, a more precise solution for the large-amplitude blade motion can be obtained with numerical techniques (e.g., Zeller et al., 2014; Zhu and Chen, 2015; Luhar and Nepf, 2016; Zhu et al., 2018; Chen and Zou, 2019, Chen and Zou, 2020b). The consistent-mass cable model described in Zhu et al. (2020b) captured an asymmetric whip-like blade motion. With accurate modeling of blade motion, the cable-model-based wave attenuation model showed a good agreement with the experiments for suspended canopies, though underestimating the wave decay coefficient by 10% (Zhu et al., 2021). However, the analytical solutions are still useful to describe the mechanisms that influence blade motion related to wave attenuation. The analytical solutions are also computationally efficient and easy to implement into large-scale models such as SWAN (Simulating WAves Nearshore, Suzuki et al., 2012).

Wave attenuation by vegetation is determined by wave conditions and vegetation characteristics, including morphological (e.g., plant/canopy density and blade length, width, and thickness) and mechanical properties (e.g., blade flexural rigidity). The vegetation characteristics depend on the growth of vegetation and therefore show a seasonal variation (Möller and Spencer, 2002; Möller, 2006; Koch et al., 2009). Most salt-marsh grasses, such as *Spartina alterniflora* (Marsooli et al., 2017), *Spartina anglica* (Schulze et al., 2019), *Spartina foliosa* (Foster-Martinez et al., 2018), *Salicornia pacific* (Foster-Martinez et al., 2018), and *Elymus athericus* (Schulze et al., 2019), contribute more wave energy dissipation during summer than winter and spring due to greater plant stem stiffness, canopy height, and aboveground biomass in summer than other seasons. Most seagrasses, such as *Ruppia maritima* (Chen et al., 2007), *Zostera marina* (Hansen and Reidenbach, 2013), and *Zostera noltii* (Paul and Amos, 2011), also show a similar pattern to dissipate more wave energy in summer with greater blade length, blade width, canopy height, and canopy density in summer than other seasons. In winter, more vegetation breaks or dies off, reducing the wave attenuation capacity (Marsooli et al., 2017; Vuik et al., 2018). Therefore, Ondiviela et al. (2014) proposed that the large, long-living, and slow-growing seagrass species (e.g., *Posidonia oceanica*) with biomass largely independent of seasonal fluctuations may provide favorable coastal protection.

Wave attenuation by kelp is also dependent on wave conditions and the morphological and mechanical properties of kelp. For example, sparse (~0.1 plants/m^2) *Macrocystis pyrifera* (giant kelp) forests was observed to have no significant effects on wave attenuation (Elwany et al., 1995). Similar results were also observed for highly flexible *Nereocystis luetkeana* (bull kelp, Gaylord et al., 2003) and deeply submerged *Ecklonia radiata* (< 10% of the water column, Morris et al., 2019). However, dense (25 plants/m^2) *Laminaria hyperborea* (tangle) in shallow water (5 m) could attenuate 70%−85% of wave energy over 258 m into the canopy along the direction of wave propagation (Mork, 1996). Unlike the wild kelp that grows on the seafloor, cultivated kelp is commonly suspended in the water column supported by a mooring system. Since the kinetic energy of intermediate and deep-water waves is concentrated near the surface, suspended kelp farms with a dense plant density are believed to dissipate more wave energy than naturally occurring kelp beds with a sparse plant density (Zhu et al., 2021). With laboratory experiments, Zhu et al. (2021) demonstrated that *Saccharina latissima* (sugar kelp) aquaculture farms with 20 longlines of 1 m-long blades and 100 blades/m at 1.1 m below the water surface have the potential to dissipate 12.5% energy of 0.35 m-high waves with the period of 6.3 s in 4 m-deep water. The wave attenuation can be further improved by planting the kelp more densely and adding more kelp longlines (Zhu et al., 2021). Cultivated kelp grows seasonally resulting in varying performances for wave attenuation, which are not fully understood. Considering seasonal variations of natural materials is essential to understand their capacity for wave attenuation, select appropriate species, and design strategies for nature-based coastal protection.

This study aims to develop an analytical wave attenuation model that resolves the blade motion and investigates the wave attenuation characteristics of submerged flexible vegetation and suspended cultivated kelp. The analytical wave attenuation model was derived by simplifying and linearizing the blade motion. The analytical model was compared with the experiments in Luhar et al. (2017) and Lei and Nepf (2019b) for submerged vegetation and the experiments in Zhu et al. (2021) for suspended kelp canopies. With the analytical model, the analytical solutions for the bulk drag coefficient and effective blade length were derived and compared with the fitted values from the experimental data. After the data-model comparison, the analytical model was then used to analyze the seasonal performance of submerged vegetation and suspended canopies for wave attenuation as well as the implications for nature-based coastal protection.

2. Theory

Various vegetation and kelp species have different morphologies, each with its own associated mechanics (Denny and Gaylord, 2002),

which influence the selection of appropriate techniques to model the dynamics of vegetation and kelp. In this study, seagrass *Zostera marina* and sugar kelp *Saccharina latissima* (common species in Maine, USA) are selected as representatives for submerged vegetation and suspended kelp, respectively (Fig. 1). *Zostera marina* is composed of roots, rhizome, sheath, and leaves (blades). There is one or several leaves fixed on the sheath. The sheath is short but much more rigid than the leaves. Sugar kelp *Saccharina latissima* consists of holdfast, stipe, and blade. The stipe of *Saccharina latissima* is very short compared to the blade but much more rigid than the blade. In the development of the wave attenuation model, the seagrass sheath and kelp stipe are considered rigid, while the seagrass leaves and kelp blade are considered flexible. The seagrass leaf and kelp blade are commonly modeled using the cantilever beam theory. For other species that have different morphologies, other methods might be considered. For example, for the kelp species with a long stipe, two dynamic models are commonly used: mass-damped-spring model for *Eisenia arborea* and *Pterygophora californica* (where the stipe is treated as a cantilever-type spring with entire effective mass concentrated at the free end of the stipe, Denny et al., 1998), and buoy-on-rope model for bull kelp *Nereocystis luetkeana* and *Macrocystis pyrifera* (where the pneumatocyst is modeled as a buoy and the stipe is modeled as a thin, straight, non-buoyant rope, Utter and Denny, 1996; Denny et al., 1997; Stevens et al., 2001; Zhu et al., 2020a). Different terminologies are used for seagrass and kelp although their physical forms are similar (Fig. 1). For the convenience of description in the model development, '(flexible) blade' is used to describe the vegetation leaf and kelp blade.

2.1. Model set-up

A three-layer model is used to derive the wave attenuation for submerged and suspended canopies (Fig. 2). The horizontal coordinate (x) is positive in the direction of wave propagation with $x = 0$ at the leading edge of the canopy and $x = L_v$ at the ending edge. The vertical coordinate (z) is positive upward with $z = 0$ at the still water level (SWL). The canopy height (d_2) is defined as the average submerged length (l) of the canopy blades. The thicknesses of the water layers above and below the canopy are d_1 and d_3, respectively. The water depth from the SWL is $h = d_1 + d_2 + d_3$, where the seafloor is located at $z = -h$ and assumed horizontal. This generalized three-layer model can be used to analyze the wave attenuation characteristics of (i) submerged ($d_1 \neq 0$ and $d_3 = 0$), (ii) emerged ($d_1 = 0$ and $d_3 = 0$), (iii) suspended ($d_1 \neq 0$ and $d_3 \neq 0$), and (iv) floating ($d_1 = 0$ and $d_3 \neq 0$) canopies.

Based on linear wave theory (Dean and Dalrymple, 1991), the frictionless horizontal wave orbital velocity (u_0) is given by

$$u_0 = \frac{H}{2}\omega\Gamma(z)\cos(kx - \omega t), \tag{1}$$

where H is the wave height, ω is the wave angular frequency, t is the time, $\Gamma(z) = \cosh k(h+z)/\sinh kh$ is the vertical decay factor, and k is the wave number obtained from the dispersion relation, $\omega^2 = gk\tanh kh$, with g the gravitational acceleration. Due to the presence of a canopy, the flow velocity in the canopy decreases and displays a phase shift relative to the flow velocity above the canopy (Lowe et al., 2005; Rosman et al., 2013; Henderson et al., 2017). For simplicity, the phase shift is not considered and the magnitude reduction is considered using a factor α_w following Lowe et al. (2005) such that the within canopy velocity can be estimated by

$$u = \alpha_w u_0, \tag{2}$$

where the factor α_w is calculated using the numerical solution in Lowe et al. (2005).

2.2. Blade motion

The flexible blade can be modeled as a cantilever beam using the cable model described in Zhu et al. (2020b, 2021), where the blade motion is governed by the balances of blade inertia, blade bending resistance, blade tension, blade weight, buoyancy, friction, and hydrodynamic force. The vertical blade displacement, geometrical nonlinearity of the blade deflection, and the vertical forces including friction, buoyancy, and tension create a difficulty to obtain analytical solutions

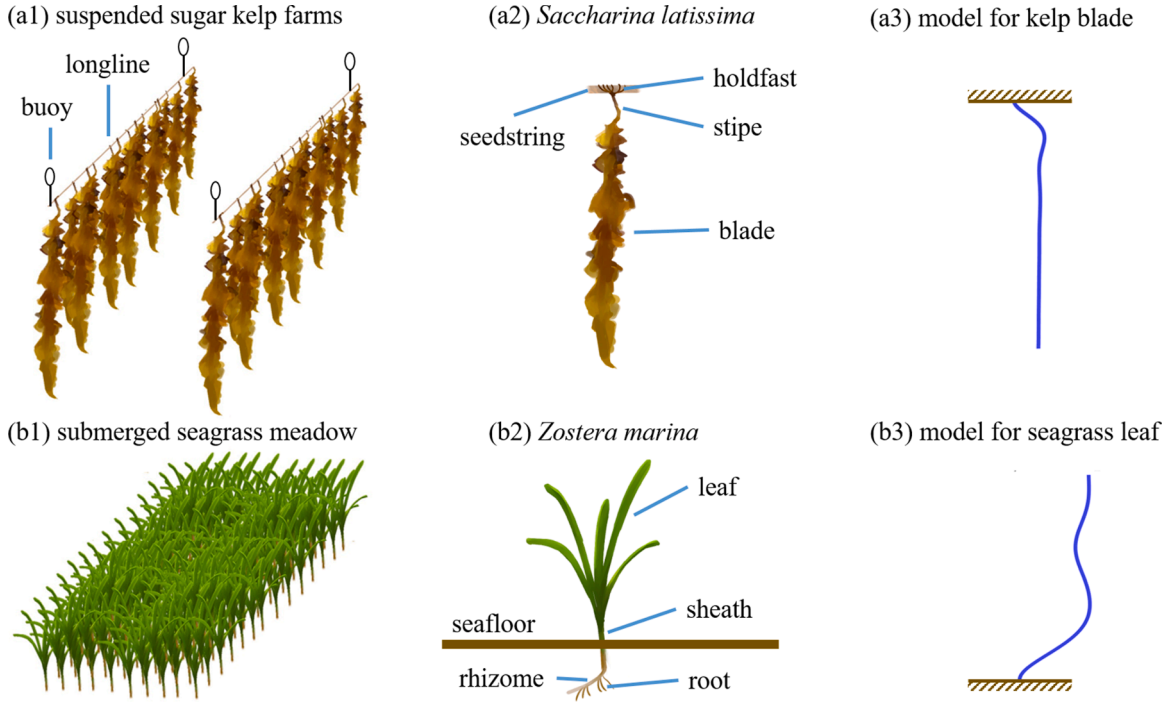

Fig. 1. Sketches of (a1) suspended sugar kelp (*Saccharina latissima*) farms, (a2) morphology of *Saccharina latissima*, (a3) cantilever-beam model for suspended blade fixed at the top end, (b1) submerged seagrass (*Zostera marina*) meadow, (b2) morphology of *Zostera marina*, (b3) cantilever-beam model for submerged blade fixed at the bottom end.

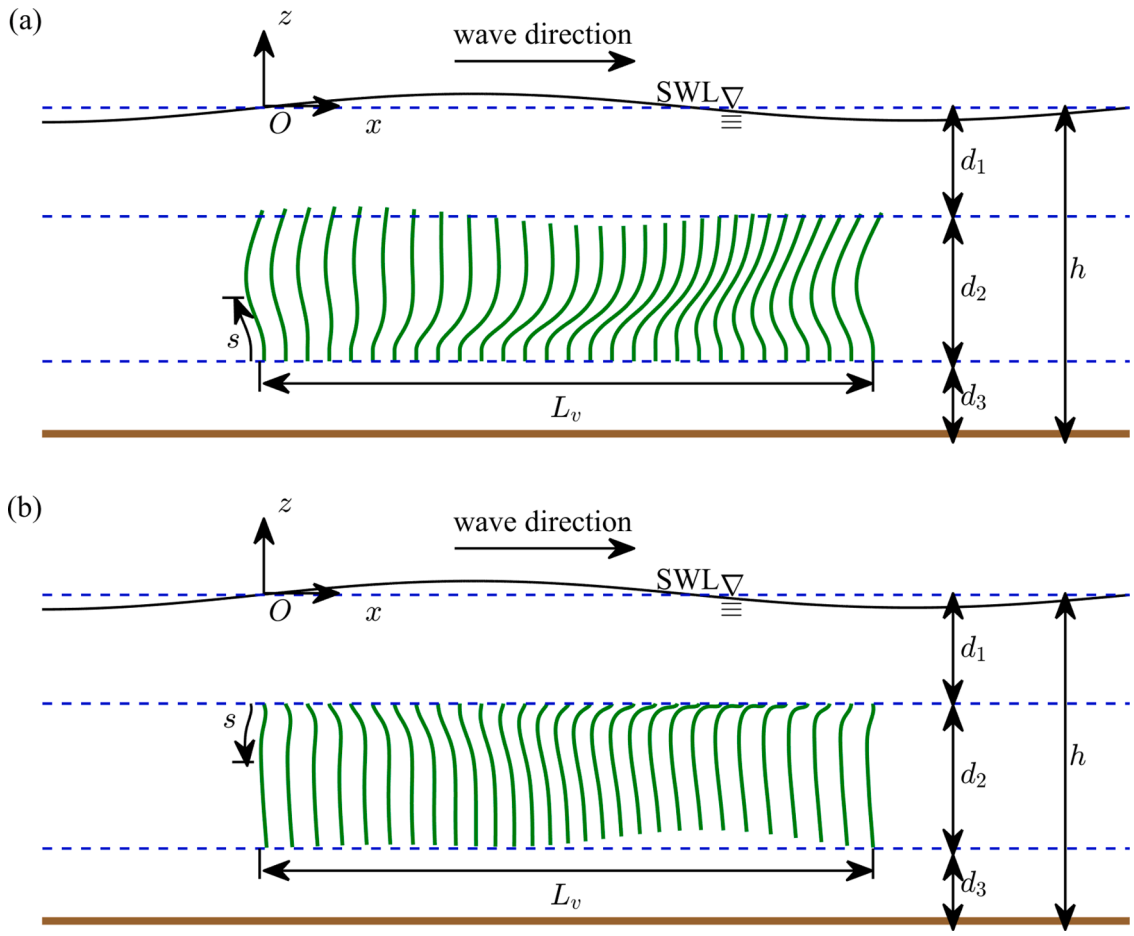

Fig. 2. Sketch of the three-layer model for wave attenuation by canopies (a) fixed at the bottom end and (b) fixed at the top end. The coordinate (x, z) is originated at the leading edge of the canopy ($x = 0$) and the still water level (SWL, $z = 0$). The distance from the fixed end of the blade is s. The canopy length is L_v and the canopy height is d_2. The thicknesses of the layers above and below the canopy are d_1 and d_3, respectively. The water depth from the SWL is $h = d_1 + d_2 + d_3$.

and therefore are neglected in this study. The effects of neglecting these terms on blade motion and wave attenuation are assessed later in Section 3.2. Thus, the governing equation for the horizontal blade displacement (ξ) is then simplified as the balance of blade inertia, blade bending resistance, and hydrodynamic force, which is expressed as

$$\rho_v A_c \ddot{\xi} + EI\xi'''' = f_x, \tag{3}$$

where ξ is a function of time (t) and the distance s along the blade length from the fixed end ($s = 0$), the dot ($\dot{}$) indicates the derivative with respect to t, the prime ($'$) indicates the derivative with respect to s, ρ_v is the blade mass density, A_c is the blade cross-section area, E is the elastic modulus, I is the second moment of the cross section, and f_x is the hydrodynamic force per unit length. The relation between s and z (Fig. 2) is

$$z = \begin{cases} -d_1 - d_2 + s, & \text{blade fixed at the bottom end,} \\ -d_1 - s, & \text{blade fixed at the top end.} \end{cases} \tag{4}$$

According to the Morison equation (Morison et al., 1950), the hydrodynamic force (f_x) is decomposed into virtual buoyancy (f_{VB}), drag (f_d), and added mass force (f_{AM}) and is given by

$$f_x = f_{VB} + f_d + f_{AM}, \tag{5}$$

with

$$f_{VB} = \rho_w A_c \dot{u}, \tag{6}$$

$$f_d = \frac{1}{2} C_d \rho_w b |u - \dot{\xi}|(u - \dot{\xi}), \tag{7}$$

and

$$f_{AM} = C_m \rho_w A_c \left(\dot{u} - \ddot{\xi}\right), \tag{8}$$

where ρ_w is the water density, b is the projected width of the blade, C_d is the drag coefficient, and C_m is the added mass coefficient. For the blade with rectangular cross section, the drag coefficient (C_d) and added mass coefficient (C_m) are

$$C_d = \max\left(10KC^{-1/3}, 1.95\right) \tag{9}$$

and

$$C_m = \min(C_{m1}, C_{m2}), \tag{10}$$

respectively, with $C_{m1} = \begin{cases} 1 + 0.35KC^{2/3}, KC < 20 \\ 1 + 0.15\ KC^{2/3}, KC \geq 20 \end{cases}$ and $C_{m2} = 1 + (KC - 18)^2/49$ (Luhar, 2012; Luhar and Nepf, 2016). In (9) and (10), $KC = u_m T/b$ is the Keulegan–Carpenter number with $T = 2\pi/\omega$ the wave period and u_m the magnitude of the water velocity relative to the blade, yielding a non-constant C_d and C_m. The formulas are fitted from the experimental data in Keulegan and Carpenter (1958) and Sarpkaya and O'Keefe (1996) for rigid flat plates in oscillatory flows with $R^2 = 0.972$ and 0.912 for C_d and C_m (Fig. 3), respectively. To obtain an analytical solution, the nonlinear drag is linearized as

$$f_d = \frac{1}{2} C_d \rho_w b |u - \dot{\xi}|(u - \dot{\xi}) \approx c(u - \dot{\xi}), \tag{11}$$

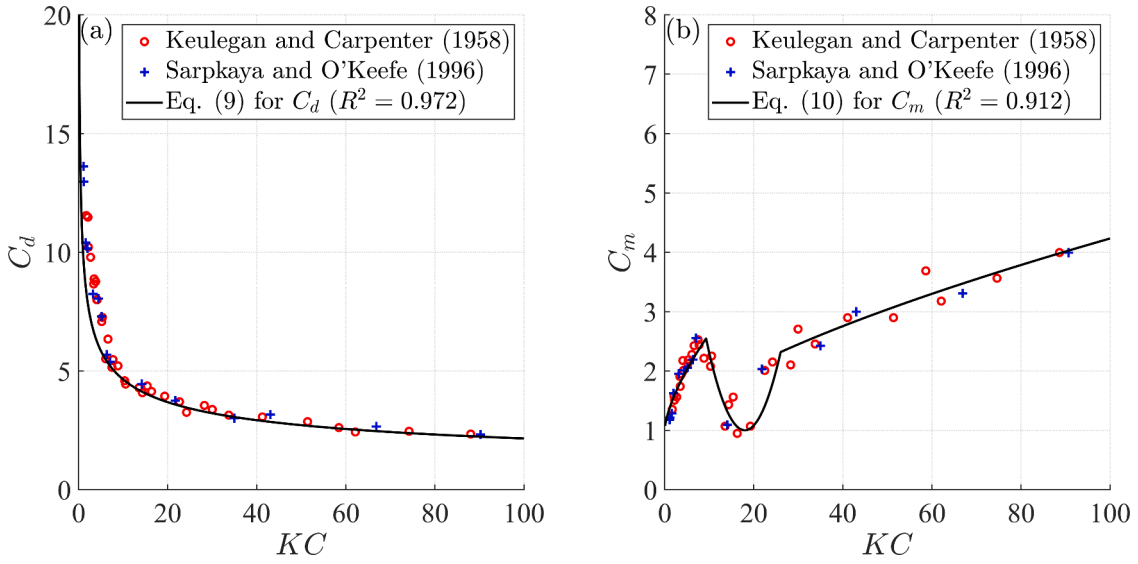

Fig. 3. (a) Drag coefficient (C_d) and (b) added mass coefficient (C_m) as a function of Keulegan–Carpenter number (KC) for rigid flat plates in oscillatory flows. The data from Keulegan and Carpenter (1958) and Sarpkaya and O'Keefe (1996) are denoted by red open circles and blue pluses, respectively. The black lines indicate the values calculated from the formulas in Luhar and Nepf (2016) and Luhar (2012) with R^2 in the legend (For interpretation of the references to color in this figure legend, the reader is referred to the web version of this article.).

where the linearization coefficient (c) is obtained from the Lorentz's condition of equivalent work (Sollitt and Cross, 1972). This requires that the nonlinear and linear drag accounts for the same amount of energy dissipation averaged over one wave period such that $\int_{-d_1-d_2}^{-d_1} \overline{\frac{1}{2}C_d\rho_w b|u-\dot{\xi}|(u-\dot{\xi})^2}dz = \int_{-d_1-d_2}^{-d_1} \overline{c(u-\dot{\xi})^2}dz$, yielding

$$c = \frac{\int_{-d_1-d_2}^{-d_1} \overline{\frac{1}{2}C_d\rho_w b|u-\dot{\xi}|(u-\dot{\xi})^2}dz}{\int_{-d_1-d_2}^{-d_1} \overline{(u-\dot{\xi})^2}dz} = \frac{1}{2}C_d\rho_w b u_{er}. \tag{12}$$

In (12), the overline indicates the time average over one wave period and the equivalent relative velocity magnitude $u_{er} = \int_{-d_1-d_2}^{-d_1} \overline{|u-\dot{\xi}|(u-\dot{\xi})^2}dz \Big/ \int_{-d_1-d_2}^{-d_1} \overline{(u-\dot{\xi})^2}dz$ The linearization coefficient (c) is equivalent to the viscous damping coefficient per unit length with the unit of [Ns/m^2]. Eq. (12) also shows that c is dependent on the equivalent relative velocity magnitude u_{er}. The linearization of the drag force in random waves is typically done using the Borgman (1967) method based on the distribution of the wave orbital velocity resulting in a different expression of the linearization coefficient in Zhu et al. (2020a).

Substituting (1), (5) with linearized drag (11) into (3) yields

$$m\ddot{\xi} + c\,\dot{\xi} + EI\xi'''' = \frac{H}{2}\omega\Gamma[c\cos(kx-\omega t) + \omega m_I \sin(kx-\omega t)], \tag{13}$$

where $m = (\rho_v + C_m\rho_w)A_c$ and $m_I = (1 + C_m)\rho_w A_c$. The boundary conditions for a cantilever beam are set as $\xi(0, t) = 0$, $\xi'(0, t) = 0$, $\xi''(l, t) = 0$, and $\xi'''(l, t) = 0$. Solving (13) with the normal mode approach (Rao, 2007) yields

$$\xi = \frac{H}{2}\Gamma[\gamma_s \sin(kx-\omega t) + \gamma_c \cos(kx-\omega t)]. \tag{14}$$

In (13), γ_s and γ_c are the transfer functions and expressed as

$$\gamma_s = \frac{\omega}{\Gamma}\sum_{n=1}^{\infty}\phi_n \frac{\omega I_n\left(\lambda_n^2 - \omega^2\right) - D_n 2\zeta_n\lambda_n\omega}{\left(\lambda_n^2 - \omega^2\right)^2 + (2\zeta_n\lambda_n\omega)^2} \tag{15}$$

and

$$\gamma_c = \frac{\omega}{\Gamma}\sum_{n=1}^{\infty}\phi_n \frac{D_n\left(\lambda_n^2 - \omega^2\right) + \omega I_n 2\zeta_n\lambda_n\omega}{\left(\lambda_n^2 - \omega^2\right)^2 + (2\zeta_n\lambda_n\omega)^2}, \tag{16}$$

where $\phi_n = (\cos\mu_n l + \cosh\mu_n l)(\sin\mu_n s - \sinh\mu_n s) + (\sin\mu_n l + \sinh\mu_n l)(\cosh\mu_n s - \cos\mu_n s)$ is the nth normal mode of the cantilever beam with μ_n the nth solution of $1 + \cos\mu l\cosh\mu l = 0$, $\lambda_n = \mu_n^2\sqrt{EI/m}$ is the nth natural frequency of the blade, $2\zeta_n\lambda_n = c/m$, $D_n = \int_0^l c\Gamma\phi_n ds \Big/ \int_0^l m\phi_n^2 ds$, and $I_n = \int_0^l m_I\Gamma\phi_n ds \Big/ \int_0^l m\phi_n^2 ds$. Since Γ is expressed in z and ϕ_n is expressed in s, the relation between s and z in (4) is required to calculate the integral $\int_0^l \Gamma\phi_n ds$. Substituting (14) into (12) yields the expression of the linearization coefficient in terms of the transfer functions,

$$c = \frac{1}{2}C_d\rho_w b\frac{H}{2}\omega\frac{8}{3\pi}\frac{\int_{-d_1-d_2}^{-d_1}\Gamma^3\left[(1+\gamma_s)^2 + \gamma_c^2\right]^{3/2}dz}{\int_{-d_1-d_2}^{-d_1}\Gamma^2\left[(1+\gamma_s)^2 + \gamma_c^2\right]dz}. \tag{17}$$

The linearization coefficient can be obtained iteratively. Starting from a static blade, an initial c is calculated from Eq. (17) by assuming $\gamma_s = 0$ and $\gamma_c = 0$. Once the transfer functions γ_s and γ_c are obtained from (15) and (16), c can be updated from (17). The procedure is repeated until a convergent solution is obtained.

2.3. Wave attenuation

The wave energy dissipation is assumed to be attributed to the work of the canopy drag following Zhu et al. (2020a) such that

$$\frac{\partial E c_g}{\partial x} = -\int_{-d_1-d_2}^{-d_1} N\alpha_c \overline{f_d(u-\dot{\xi})}dz, \tag{18}$$

where $E = \rho_w g H^2/8$ is the local wave energy per unit horizontal area, $c_g = \omega(1 + 2kh/\sinh 2kh)/2k$ is the wave group velocity, N is the canopy

density defined as the number of blades per unit horizontal area, and $\alpha_\varepsilon \leq 1$ is a factor to consider the sheltering effects between blades with α_ε=1 for no sheltering. The factor α_ε is calibrated through experiments. Substituting the quadratic drag force (7) into (18) yields the transmitted wave height at distance x in relation to the incident wave height H_0 at $x = 0$,

$$\frac{H(x)}{H_0} = \frac{1}{1 + k_D H_0 x}, \tag{19}$$

where the wave decay coefficient (k_D) is expressed as

$$k_D = \frac{4\alpha_\varepsilon C_d b N k^2}{3\pi \sinh kh(2kh + \sinh 2kh)} \int_{-d_1-d_2}^{-d_1} \left[\sqrt{(1+\gamma_s)^2 + \gamma_c^2}\right]^3 \cosh^3 k(h+z)dz. \tag{20}$$

It should be noted that Eq. (19) is obtained using quadratic drag. Using the linearized drag (11) yields an exponential decayed wave height as $H = H_0 e^{-k_D H_0 x}$, which is also often used in practice (e.g., Kobayashi et al., 1993; Méndez et al., 1999; Zhu and Zou, 2017). The two wave decay forms are linked through a piecewise method (Appendix C of Zhu, 2020). The piecewise function method indicates that the exponential decay form with linearized drag would overestimate the wave attenuation. Therefore, the fractional decay form in (19) is recommended (Zhu, 2020). However, for weak wave attenuation such that $k_D H_0 x < 0.5$, the difference between $1/(1 + k_D H_0 x)$ and $e^{-k_D H_0 x}$ is less than 10%.

For the canopies with unsheltered rigid blades such that $\alpha_\varepsilon = 1$, $\gamma_s = 0$, and $\gamma_c = 0$, the solution (20) reduces to the solution in Zhu and Zou (2017), i.e.,

$$k_{D,R} = \frac{C_d b N k}{9\pi} \frac{9\sinh k(d_2+d_3) - 9\sinh k d_3 + \sinh 3k(d_2+d_3) - \sinh 3k d_3}{\sinh kh(2kh + \sinh 2kh)}. \tag{21}$$

For bottom rooted vegetation such that $d_3 = 0$, solution (21) can be further reduced to the solutions by Dalrymple et al. (1984) and Kobayashi et al. (1993). For shallow water waves with $kh < 0.1\pi$, (21) reduces to

$$k_{D,R} = \frac{C_d b N k l}{3\pi h^2}, \tag{22}$$

indicating that the wave decay coefficient is proportional to the drag coefficient, canopy density, blade width, and blade length, but inversely proportional to the wavelength and the square of water depth. Thus, the wave attenuation decreases more dramatically with increasing water depth than other parameters for shallow water waves. According to (22), the wave attenuation is independent from the vertical position of the canopy since the horizontal wave orbital velocity minimally decays to the bottom.

2.4. Bulk drag coefficient and effective blade length

According to (18), the wave dissipation ratio is proportional to $\int_{-d_1-d_2}^{-d_1} \overline{f_d(u-\dot{\xi})}dz \propto \int_0^l \overline{C_d|u_r|^3}ds$ with $u_r = u - \dot{\xi}$ the relative velocity. Obtaining the wave dissipation ratio requires computation of the relative velocity, in order to consider the wave-blade interaction. To reduce the computation for the relative velocity including resolving the blade motion, the bulk drag coefficient and effective blade length methods

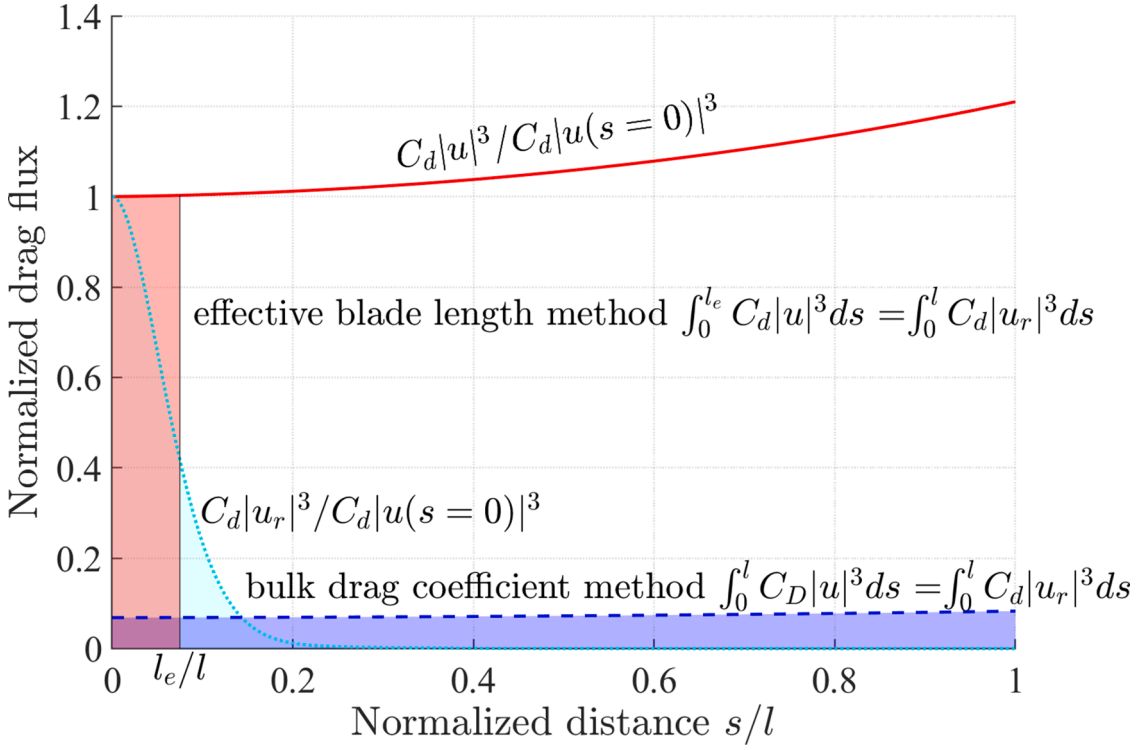

Fig. 4. Concept sketch for bulk drag coefficient (C_D) and effective blade length (l_e) methods. The bulk drag coefficient method is denoted by the blue patch such that the area of the blue patch is equal to the area under the cyan line with $\int_0^l C_D|u|^3ds = \int_0^l C_d|u_r|^3ds$, where u is the within canopy wave orbital velocity, u_r is the relative velocity between the blade and flow, C_d is the original drag coefficient, s is the distance along the blade length, and l is the blade length. The effective blade length method is denoted by the red patch such that the area of the red patch is equal to the area under the cyan line with $\int_0^{l_e} C_d|u|^3ds = \int_0^l C_d|u_r|^3ds$ (For interpretation of the references to color in this figure legend, the reader is referred to the web version of this article.).

with a rigid blade assumption are often used, especially for implementation into large-scale models. The bulk drag coefficient (C_D) is a reduced drag coefficient such that $\int_0^l C_D|u|^3 ds = \int_0^l C_d|u_r|^3 ds$ while the effective blade length (l_e) is a reduced blade length such that $\int_0^{l_e} C_d|u|^3 ds = \int_0^l C_d|u_r|^3 ds$ (Fig. 4). Traditionally, C_D and l_e are calibrated with experiments or numerical models. However, with the analytical model developed in Section 2.3, analytical solutions for C_D and l_e can be obtained.

To derive the solution for the bulk drag coefficient, replacing C_d in (21) by C_D and substituting the result into (20) yields

$$C_D = \frac{12k\alpha_\varepsilon \int_{-d_1-d_2}^{-d_1} \cosh^3 k(h+z)\left[\sqrt{(1+\gamma_s)^2+\gamma_c^2}\right]^3 dz}{9\sinh k(d_2+d_3) - 9\sinh kd_3 + \sinh 3k(d_2+d_3) - \sinh 3kd_3} C_d. \quad (23)$$

For shallow water waves with $kh < 0.1\pi$, (23) reduces to

$$C_D = \frac{\alpha_\varepsilon}{d_2} \int_{-d_1-d_2}^{-d_1} \left[\sqrt{(1+\gamma_s)^2+\gamma_c^2}\right]^3 dz C_d. \quad (24)$$

To derive the solution for the effective blade length, replacing d_2 in (21) by l_e and substituting the result into (20) yields

$$9\sinh k(l_e+d_3) + \sinh 3k(l_e+d_3) = 9\sinh kd_3 + \sinh 3kd_3 + 12k\alpha_\varepsilon \int_0^l \cosh^3 k(h+z)\left[\sqrt{(1+\gamma_s)^2+\gamma_c^2}\right]^3 ds. \quad (25)$$

For submerged vegetation with $d_3 = 0$, (25) reduces to

$$9\sinh kl_e + \sinh 3kl_e = 12k\alpha_\varepsilon \int_0^l \cosh^3 k(h+z)\left[\sqrt{(1+\gamma_s)^2+\gamma_c^2}\right]^3 ds. \quad (26)$$

When l_e is far less than the wave length with $kl_e < 0.1\pi$, (26) reduces to

$$l_e = \alpha_\varepsilon \int_0^l \cosh^3 k(h+z)\left[\sqrt{(1+\gamma_s)^2+\gamma_c^2}\right]^3 ds. \quad (27)$$

For shallow water waves with $kh < 0.1\pi$, (25) reduces to

$$l_e = \alpha_\varepsilon \int_0^l \left[\sqrt{(1+\gamma_s)^2+\gamma_c^2}\right]^3 ds. \quad (28)$$

Dividing (24) by (28) yields

$$\frac{l_e}{l} = \frac{C_D}{C_d}, \quad (29)$$

indicating that the "rate of blade length reduction" is equal to the "rate of drag coefficient reduction" in shallow water waves. These reductions reflect the decreases in wave attenuation resulting from the blade motion. Eq. (29) holds because the wave decay coefficient of rigid canopies is proportional to the drag coefficient and blade length in shallow water waves as shown in (22).

3. Results

3.1. Model-data comparison

3.1.1. Experimental data description

The analytical model was compared with the experiments in Luhar et al. (2017) and Lei and Nepf (2019b) for submerged vegetation and the experiments in Zhu et al. (2021) for suspended kelp canopies. In the experiments for submerged vegetation (Luhar et al., 2017; Lei and Nepf, 2019b), the artificial vegetation consisted of six 13 cm-long, 0.3 cm-wide, and 0.1 mm-thick flexible blades (to model seagrass leaves) and one 1 cm-long solid wood cylinder (to model seagrass sheath). The diameters of the wood cylinders were 7.8 mm in Luhar et al. (2017) and 6.9 mm in Lei and Nepf (2019b). The flexible blades were made from low-density polyethylene (LDPE) film with $\rho_v = 0.92$ g/cm^3 and $E = 0.3$ GPa. The blades were located separately such that the sheltering factor $\alpha_\varepsilon = 1$. The canopy density was 280 to 1800 stems/m^2 with 1680 to 10,800 blades/m^2. The canopy lengths were 5 m in Luhar et al. (2017) and 3.5–7 m in Lei and Nepf (2019b). The wave height was 1 to 11.2 cm, the wave period was 0.8 to 2 s, and the water depth was 16 to 45 cm. Thus, the dimensionless parameters are $kh = 0.44 - 2.7$, $l/h = 0.29 - 0.8$, $KC = 9 - 135$, $Ca = 64 - 3796$, $L = 2 - 30$, and $\gamma = 0.16 - 0.30$, where $Ca = \rho_w b u_m^2 l^3/EI$ is the Cauchy number, $L = l\omega/u_m$ is the ratio of the blade length to the wave excursion (u_m/ω), and $\gamma = \beta S^{-1/2}$ with $\beta = \frac{g(\rho_w-\rho_v)A_cT}{0.5\rho_w C_d l b u_m}$ the dimensionless buoyancy defined in Henderson (2019) and $S = \frac{EIT}{0.5\rho_w C_d l^4 b u_m}$ the dimensionless stiffness defined in Mullarney and Henderson (2010) and Henderson (2019). The value of γ determine the importance of buoyancy relative to stiffness with $|\gamma| < 1$ indicating buoyancy is less important than stiffness and $|\gamma| > 1$ indicating buoyancy is more important than stiffness. Details of the experiments for the submerged vegetation can be found in Luhar et al. (2017) and Lei and Nepf (2019b).

In the experiments for suspended kelp canopies, the kelp blade was modeled using silicon film with $\rho_v = 1.2$ g/cm^3 and $E = 2.04$ MPa. The model blade was 10.16 cm long, 0.95 cm wide, and 0.1 mm thick. The suspended kelp canopy consisted of 20 rows of blades, and the rows were 20 cm apart. For each row, there were 31 aggregates of blades with one aggregate/cm. For each aggregate, ten blades were fixed together at the top end of the blades. The fixed part of the blade was $l_r = 0.5$ cm, while the flexible (free) part was $l_f = 9.66$ cm. The fixed part of the blades was used to model the effects of stipes. The sheltering effects between the blades in an aggregate were considered using a sheltering factor $\alpha_\varepsilon = 0.630$. The canopy length was 3.8 m, and the canopy density was 526.3 aggregates/m^2 with 5263 blades/m^2. Three vertical positions of the suspended canopy beneath the still water level with $d_1 = 6$, 11, and 16 cm were compared in the experiments. The incident wave height was 1.8 to 3.8 cm, wave period was 0.8 to 2 s, and water depth was 30 to 40 cm with $kh = 0.58 \sim 2.33$, $l_f/h = 0.24 - 0.32$, $KC = 4.4 - 18.8$, $Ca = 9667 - 43,406$, $L = 3.4 - 14.4$, and $\gamma = -5.16 - -2.79$. The details of

Table 1
Canopy characteristics and wave conditions.

	Canopy characteristics	Wave conditions
Submerged vegetation in Luhar et al. (2017) and Lei and Nepf (2019b)	LDPE blade (0.92 g/cm^3, 0.3 GPa):13 cm long, 0.3 cm wide, 0.1 mm thick; Wood cylinder: 1 cm tall with diameter of 6.9 to 7.8 mm; Canopy density: 280-1800 stems/m^2 with 1680-10,800 blades/m^2; Fixed at the bottom end of the blade; Sheltering factor: $\alpha_\varepsilon = 1$.	Water depth: 16–45 cm Wave height: 1–11.2 cm Wave period: 0.8–2 s Wave length: 0.90–3.88 m
Suspended kelp canopies in Zhu et al. (2021)	Silicon film blade (1.2 g/cm^3, 2.04 MPa): flexible part was 9.66 cm long, 0.95 cm wide, and 0.1 mm thick; rigid part was 0.5 cm long and 0.95 cm wide; Canopy density: 526.3 aggregates/m^2 and 5263 blades/m^2; Fixed at the top end of the blade with $d_1 = 6$, 11, 16 cm below the still water line; Sheltering factor: $\alpha_\varepsilon = 0.630$.	Water depth: 30–40 cm Wave height: 1.8–3.8 cm Wave period: 0.8–2 s Wave length: 1.03–3.70 m

the experiments can be found in Zhu et al. (2021). The canopy characteristics and wave conditions are also summarized in Table 1.

3.1.2. Comparisons for wave attenuation

The analytical wave attenuation model developed in this work is compared with the experiments in Luhar et al. (2017) and Lei and Nepf (2019b) for submerged vegetation and the experiments in Zhu et al. (2021) for suspended kelp. To evaluate the performance of the analytical model, the calculations using the numerical model in Zhu et al. (2021) are also presented.

The comparisons for the wave height decay along the canopy are shown in Fig. 5. The measured wave height is featured with oscillations along the canopy. The oscillation reflects the partially standing wave induced by the wave reflection and therefore is spatially periodic with the period of the scale of half-wavelength (Luhar et al., 2017). The analytical results are similar to the numerical results for the cases in Fig. 5(a,c). But for the cases in Fig. 5(b,d), the analytical model demonstrates a smaller wave decay than the numerical model. This is because the simplification of the analytical model ignored the effects of the buoyancy, tension, and geometrical nonlinearity, which will be discussed in Section 3.2.

To evaluate the overall performance of the analytical model, the analytically and numerically calculated wave decay coefficients k_D are compared with the experimental data in Fig. 6. The numerical results show an underestimation of 11.7% (calculated using the slope of the linear fitted line between the calculated and measured values, the same hereinafter) with the normalized root mean square error, NRMSE = 0.063 (Fig. 6a). The normalization is calculated using the range (defined as the maximum value minus the minimum value) of the measured data. Compared to the numerical model, the analytical model underestimates the wave decay coefficient by 27% (Fig. 6b). However, the NRMSE of the analytical model is smaller at 0.054, indicating that the analytical model has a similar and even higher precision than the numerical model in calculating the wave attenuation.

3.1.3. Bulk drag coefficient and effective blade length

Bulk drag coefficient and effective blade length methods are simple ways to consider the effects of blade motion on wave attenuation. The values of C_D and l_e are for the flexible part of the blade with a length of l_f. In this section, the analytical solutions for C_D (23) and l_e (25) are presented and compared with the experiments in Luhar et al. (2017) and Lei and Nepf (2019b) for submerged canopies as well as the experiments in Zhu et al. (2021) for suspended canopies.

The analytically calculated C_D is compared with the fitted and measured C_D in Fig. 7, where C_D is expressed as a function of KC. Since KC does not include all the parameters governing the blade motion, such as blade flexural rigidity, the blade motions with different flexural rigidities might be different, yielding different values of C_D although with the same KC. Thus, C_D is scattered, especially for the submerged vegetation dataset with more cases and wave conditions, resulting in varying blade motion (Fig. 7c). For KC-based C_D, the analytically calculated C_D has a larger NRMSE of 0.258 than the fitted C_D with NRMSE = 0.181 for the suspended kelp canopy (Fig. 7a). Similarly, for submerged vegetation (Fig. 7c), the NRMSE of the analytically calculated C_D is 0.278, which is larger than the fitted C_D with NRMSE = 0.191. In the comparisons for the wave decay coefficient (Fig. 7b,d), the NRMSE of the k_D calculated using the analytically calculated C_D are 0.187 for the suspended kelp and 0.054 for the submerged vegetation, which are larger than those k_D calculated using the fitted C_D with NRMSE = 0.070 for the suspended kelp and 0.051 for the submerged vegetation.

The analytically calculated effective blade length of the flexible part of the blade ($l_{f,e}$) is compared with the measured and fitted $l_{f,e}$ as well as the empirical formula in Lei and Nepf (2019b) in Fig. 8, where $l_{f,e}$ is expressed as a function of CaL. In the selected experiments, the ratio of

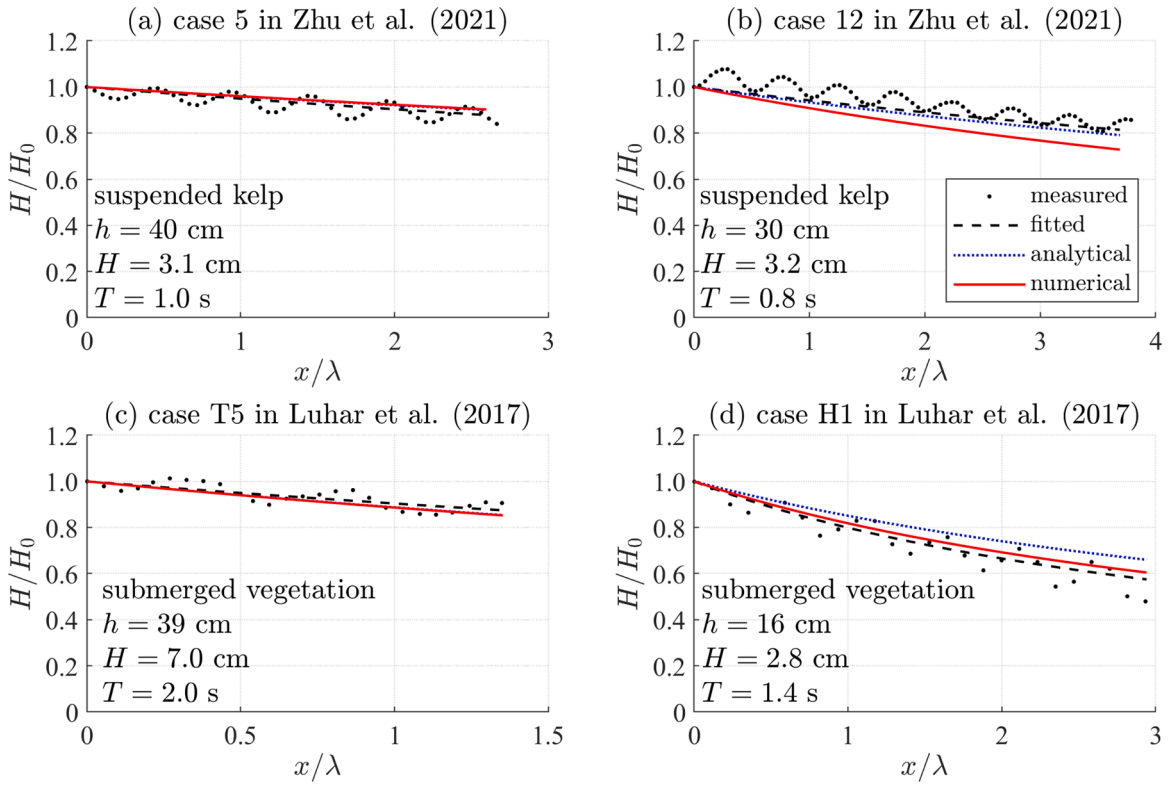

Fig. 5. Measured and calculated wave heights along (a and b) suspended kelp and (c,d) submerged vegetation. The wave height (H) is normalized by the incident wave height (H_0) and the distance (x) from the leading edge of the canopy is normalized by the canopy length (L_v). The wave conditions including water depth (h), wave height (H) and wave period (T) for the selected cases are shown on the figure. The oscillation of the measured wave height indicates the partially standing wave caused by the reflected waves.

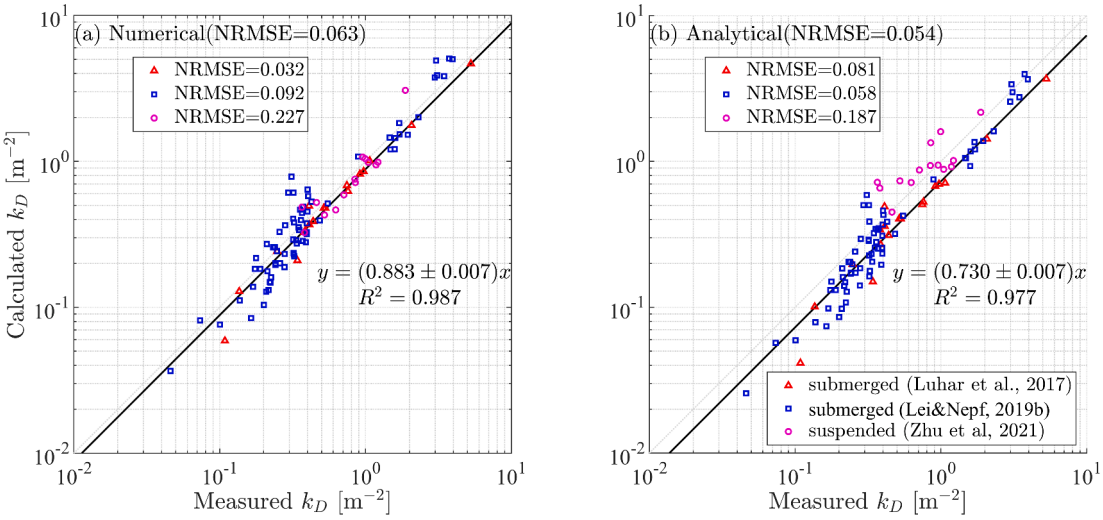

Fig. 6. (a) Numerically and (b) analytically calculated wave decay coefficients k_D compared to the experimental data from Luhar et al. (2017, red triangles), Lei and Nepf (2019b, blue squares), and Zhu et al. (2021, magenta circles) for submerged and suspended canopies. The solid black lines are the linear fits for the comparisons with expressions and R^2 nearby. The normalized root mean square error (NRMSE) by the range of measured k_D is shown in the legend (For interpretation of the references to color in this figure legend, the reader is referred to the web version of this article.).

the blade length to the wave excursion was $L > 2.0$ and the Cauchy number was $Ca > 64$. For $Ca \gg 1$ and $L \gg 1$, the effective blade length can be scaled as $\frac{l_{f,e}}{l_f} \sim (CaL)^{-1/4} l_{f,e}/l_f \sim (CaL)^{-1/4}$ by assuming the static balance between the drag and stiffness (Luhar and Nepf, 2016). For $L \ll 1$, the effective blade length can be scaled as $\frac{l_{f,e}}{l_f} \sim Ca^{-1/3} l_{f,e}\ /l_f \sim Ca^{-1/3}$ (*****Luhar and Nepf, 2011). However, Luhar et al. (2017) and Lei and Nepf (2019b) have shown that the scaling with $(CaL)^{-1/4}$ works better for the present experiments. Based on the measured horizontal forces of a single flexible blade with a wide range of CaL from 0.292 to 1.88 $\times$ 10^4, Lei and Nepf (2019b) developed the empirical formula for effective blade length given by

$$\frac{l_{f,e}}{l_f} = 0.94(CaL)^{-0.25}, \tag{30}$$

where the effective blade length is defined as the reduced length of a rigid blade that provide the same horizontal force as the flexible blade with the full length. Although this formula is developed based on the horizontal force of a single blade, it shows a good comparison with the measured $l_{f,e}$ (NRMSE=0.224, Fig. 8c) and performs well for calculating the decay coefficient k_D (NRMSE=0.050, Fig. 8d). Similar to KC-based C_D, CaL also does not include all the parameters governing the blade motion. Therefore, there might be several values of $l_{f,e}$ for different blade motions with the same CaL, resulting in scattered $l_{f,e}$, especially for the submerged vegetation experimental data with numerous types of blade motions Fig. 8c). As the range of $CL = 1678 - 10, 444$ for the wave attenuation experiments is small, the scattering of the data is more obvious. For CaL-based $l_{f,e}$, the analytically calculated $l_{f,e}$ has a larger NRMSE of 0.452 than the fitted $l_{f,e}$ with NRMSE=0.258 for suspended kelp canopies. For submerged vegetation, the NRMSEs are 0.205 for the fitted $l_{f,e}$, 0.224 of the calculated $l_{f,e}$ with the empirical formula ((30), and 0.292 for the calculated $l_{f,e}$ using the present analytical model (Fig. 8c). For the comparisons for the wave decay coefficients by suspended kelp (Fig. 8b), the NRMSE of the k_D calculated using the analytically calculated $l_{f,e}$ are 0.187, which is larger than the k_D calculated using the fitted $l_{f,e}$ with NRMSE = 0.107. However, for submerged vegetation (Fig. 8d), the NRMSE of the k_D calculated using the analytically calculated $l_{f,e}$ is 0.054, which is smaller than the k_D calculated using the fitted $l_{f,e}$ with NRMSE = 0.067. The analytically calculated $l_{f,e}$ shows a similar NRMSE to the empirical formula in Lei and Nepf (2019b) for calculating k_D with NRMSE of 0.050 (Fig. 8d).

3.2. Blade dynamics and the simplified analytical wave attenuation model

Blade dynamics have a significant influence on wave attenuation performance. To investigate the effects of blade motion on wave attenuation, the blade postures, relative velocities (u_r), and drag force flux ($f_d u_r$) are analyzed based on the simplified analytical solutions and nonlinear numerical solutions. The wave energy dissipation is determined by the drag flux ($f_d u_r \propto |u_r|^3$) as shown in (18), which is proportional to the cube of the relative velocity. The blade is so flexible that the free tip moves passively with the wave flow (Fig. 9a1,b1), resulting in a small relative velocity u_r (Fig. 9a2,a3,b2,b3). Thus, the blade segments near the free tip have little contribution to the wave dissipation. Take the submerged blade in Fig. 9b as an example, the blade segments with $s > 0.24l$ have a small relative velocity $|u_r| < 0.4\max(|u_r|)$ (Fig. 9b2) and therefore a small drag flux $\overline{f_d u_r} < 5\%\max(\overline{f_d u_r})$ (Fig. 9b4), indicating little contribution to the wave dissipation. In other words, for the flexible blade, only the blade segments near the fixed end ($s < 0.19l$ for the suspended blade in Fig. 9a and $s < 0.24l$ for the submerged blade in Fig. 9b) contribute to the wave dissipation. This is different from a rigid blade that can dissipate wave energy along the whole blade length. The blade segments near the fixed end contribute the most (>95%) wave dissipation, which builds the foundation for the effective blade length method. Therefore, accurate simulations of the dynamics of the blade segments near the fixed end are important to evaluate the wave dissipation.

The analytical model shows a symmetric motion (Fig. 9a1,b1) due to neglecting the vertical wave orbital velocity and the phase lag induced by blade displacement. The analytical model also neglected the vertical blade displacement, geometrical nonlinearity of the blade deflection, and vertical forces, including friction, buoyancy, and tension. By considering all the forces and nonlinearity, the numerical model better simulates the blade motion by capturing the asymmetric whip-like motion (Fig. 9a1,b1). The asymmetry also reflects the phase shift of the relative velocity (u_r) along the blade length (Fig. 9a3,b3). Although the analytically calculated displacements of the segments near the tip are much smaller than those calculated from the numerical model, the discrepancy between these calculations for the blade displacements

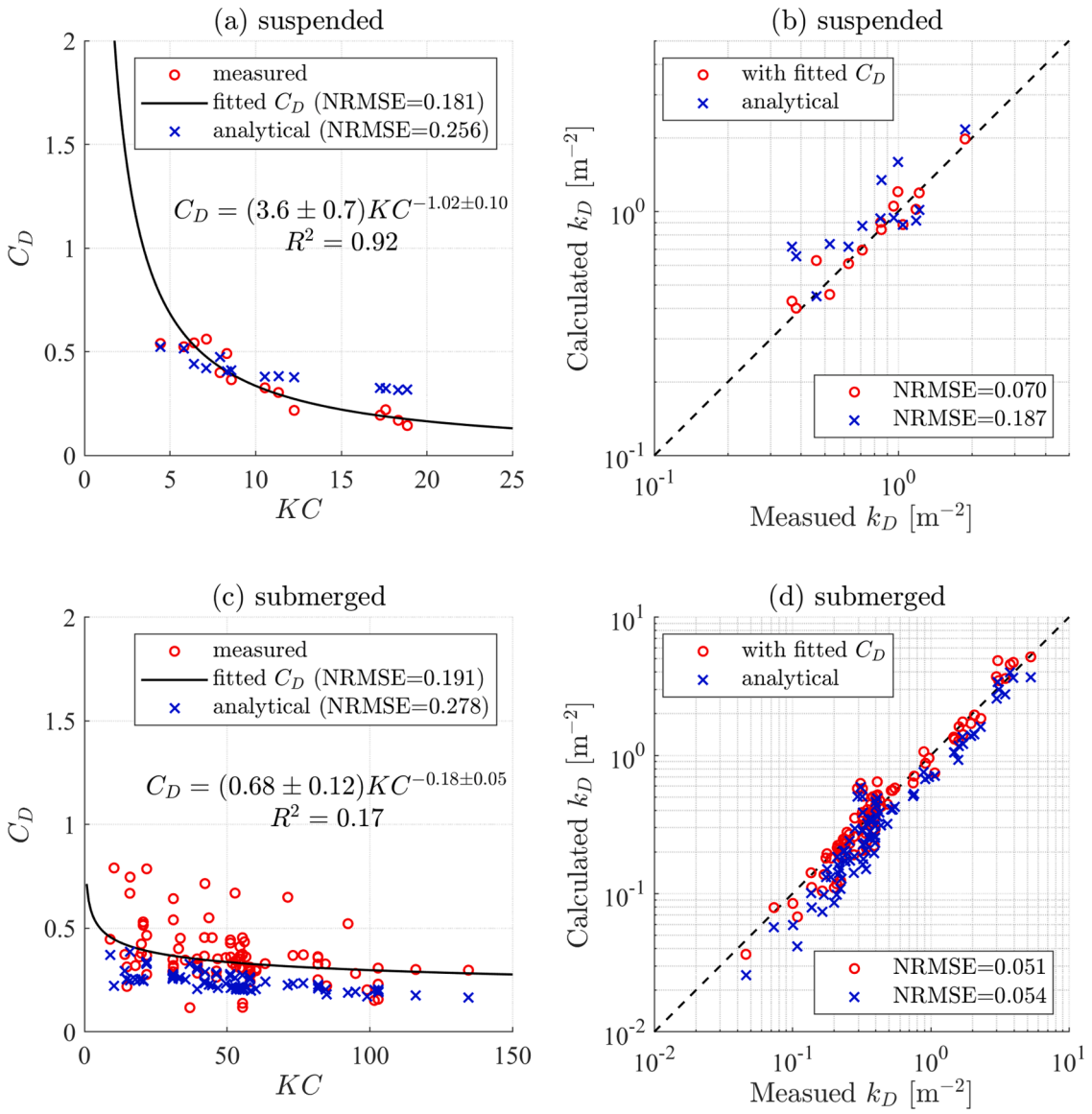

Fig. 7. Comparisons for the bulk drag coefficients (C_D) of the flexible part of the blade between the measured (red circles), analytically calculated (blue crosses), and the fitted value (black line) for (a) suspended and (c) submerged canopies. C_D is expressed as a function of Keulegan–Carpenter number (KC). Comparisons for the decay coefficient (k_D) calculated using the fitted C_D (red circles) and the analytically calculated C_D (blue crosses) for (b) suspended and (d) submerged canopies. The measured data are from Luhar et al. (2017) and Lei and Nepf (2019b) for submerged canopies and from Zhu et al. (2021) for suspended canopies. The normalized root mean square error (NRMSE) by the range of measured k_D is shown in the legend (For interpretation of the references to color in this figure legend, the reader is referred to the web version of this article.)

becomes smaller along the blade length toward the fixed end (Fig. 9a1, b1). Thus, the analytical model predicts a similar drag force flux to the numerical model (Fig. 9a4,b4) for the segments near the fixed end. However, above this region, the analytical model underestimates the drag force flux and therefore underestimates the wave attenuation (Fig. 6).

To quantify the effects of the simplifications and linearization of the blade motion in the development of the analytical wave attenuation model, the wave decay coefficient calculated from the analytical model is compared with that calculated from the numerical model using the ratio α_M defined as

$$\alpha_M = \left(k_{D,f}\right)_{\text{numerical}} \Big/ \left(k_{D,\,f}\right)_{\text{analytical}}, \tag{31}$$

where $k_{D,f}$ is the wave decay coefficient of the flexible blades without rigid sheaths or stipes such that $k_{D,f} = k_D - k_{D,r}$ with k_D the wave decay coefficient of the canopy and $k_{D,r}$ the wave decay coefficient of the rigid sheaths or stipes, and the subscript 'numerical' and 'analytical' indicate the values are calculated numerically and analytically, respectively. For the cases in this study, the ratio α_M showed the following relations with the normalized blade motion amplitude at the blade tip by the blade length (ξ_{ml}/l), i.e.,

$$\alpha_M = (0.20 \pm 0.03)\left(\frac{\xi_{ml}}{l}\right)^{-0.50\pm0.04}, \quad 0.015 \le \frac{\xi_{ml}}{l} \le 0.155 \tag{32}$$

with R^2=0.933 for suspended kelp (Fig. 10a) and

$$\alpha_M = (0.92 \pm 0.03)\left(\frac{\xi_{ml}}{l}\right)^{-0.216\pm0.014}, \quad 0.039 \le \frac{\xi_{ml}}{l} \le 0.449 \tag{33}$$

with R^2=0.863 for submerged vegetation Fig. 10b). Since the numerical results reduce to the analytical results when $\xi_{ml}/l \ll 1$, α_M approaches to 1 as ξ_{ml}/l approaching to 0. Unfortunately, formulas ((32) and (33) cannot capture this trend due to limited data. Therefore, (32) and (33)

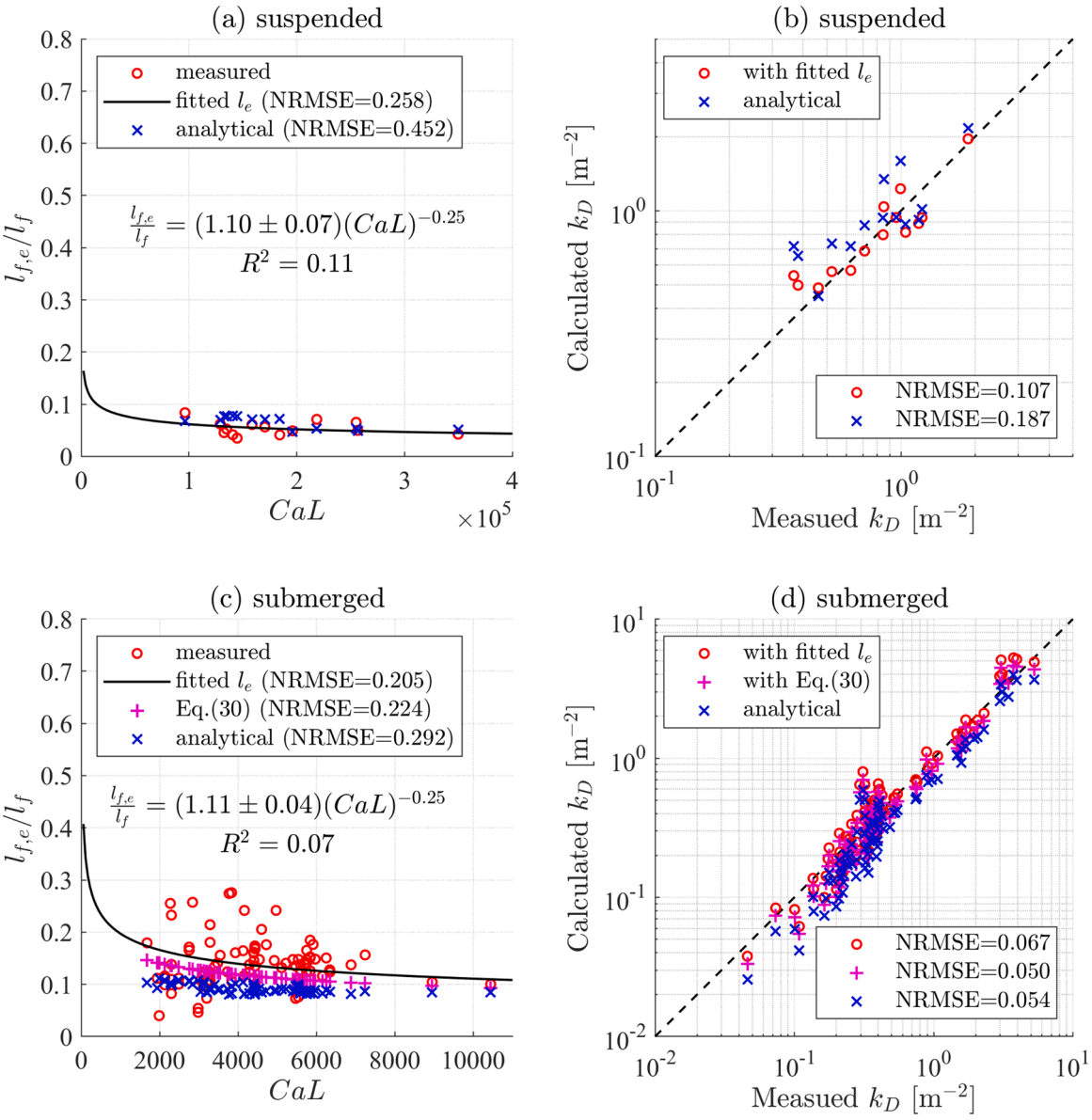

Fig. 8. Comparisons for the normalized effective blade length ($l_{f,e}/l_f$) of the flexible part of the blade (l_f) between the measured (red circles), calculated using the analytical solution (25) (blue crosses), calculated using (30), the empirical formula in Lei and Nepf (magenta pluses, 2019b), and the fitted value (black line) for (a) suspended and (c) submerged canopies. In (a) and (c), *Ca* is the Cauchy number and *L* is the ratio of the blade length to the wave excursion. Comparisons for the decay coefficient (k_D) calculated by the fitted $l_{f,e}$ (red circles), the empirical formula in Lei and Nepf (red pluses, 2019b), and the analytically calculated $l_{f,e}$ (blue crosses) for (b) suspended and (d) submerged canopies. The measured data are from Luhar et al. (2017) and Lei and Nepf (2019b) for submerged canopies and from Zhu et al. (2021) for suspended canopies. The normalized root-mean-square error (NRMSE) by the range of measured k_D is shown in the legend (For interpretation of the references to color in this figure legend, the reader is referred to the web version of this article.).

are limited to apply for the given range of ξ_{ml}/l. To address this issue, an improved formula for α_M will be developed with more data in the future. With the ratio α_M, the analytical model can be modified by multiplying the modification factor α_M. The modified analytical results underestimate the wave decay coefficient by only 10.1% (Fig. 10c), while the original analytical results underestimate the wave decay coefficient by 27% (Fig. 6b). The modification improved the analytical wave attenuation model by reducing the underestimation by (27 − 10.1)/27 = 62.6%. However, the NRMSE increased 22.2% to 0.066 (Fig. 10c) from 0.054 (Fig. 6b).

3.3. Case study for wave attenuation in different seasons

The analytical model is then used to investigate the seasonal wave attenuation capacity of kelp farms compared with seagrass meadow over one year. To represent the seagrass and kelp, *Zostera marina* (eelgrass) and *Saccharina latissima* (sugar kelp) are used, which are common species at the coast of Maine in the USA.

Regarding the parameters of seagrass, the designed length of the seagrass leaf follows the measured data in Gaeckle and Short (2002) for the *Zostera marina* at coastal Maine, USA (Fig. 11a). The corresponding leaf width and thickness as well as the length and width of the sheaths are calculated using the relationship formulas in Abdelrhman (2007) and shown in Fig. 11a. The designed mass density and elastic modulus are 700 kg/m^3 (Abdelrhman, 2007) and 0.26 GPa (Fonseca et al., 2007), respectively. The designed density is 335 shoots/m^2, and the leaf number is 3 for each shoot, such that the density is 1005 leaves/m^2 (Mattila et al., 1999). The water depth for the seagrass is designed as 5 m. For the seagrass in this case study, $\gamma = 0.04 - 0.16$, indicating that the effects of buoyancy are small and negligible.

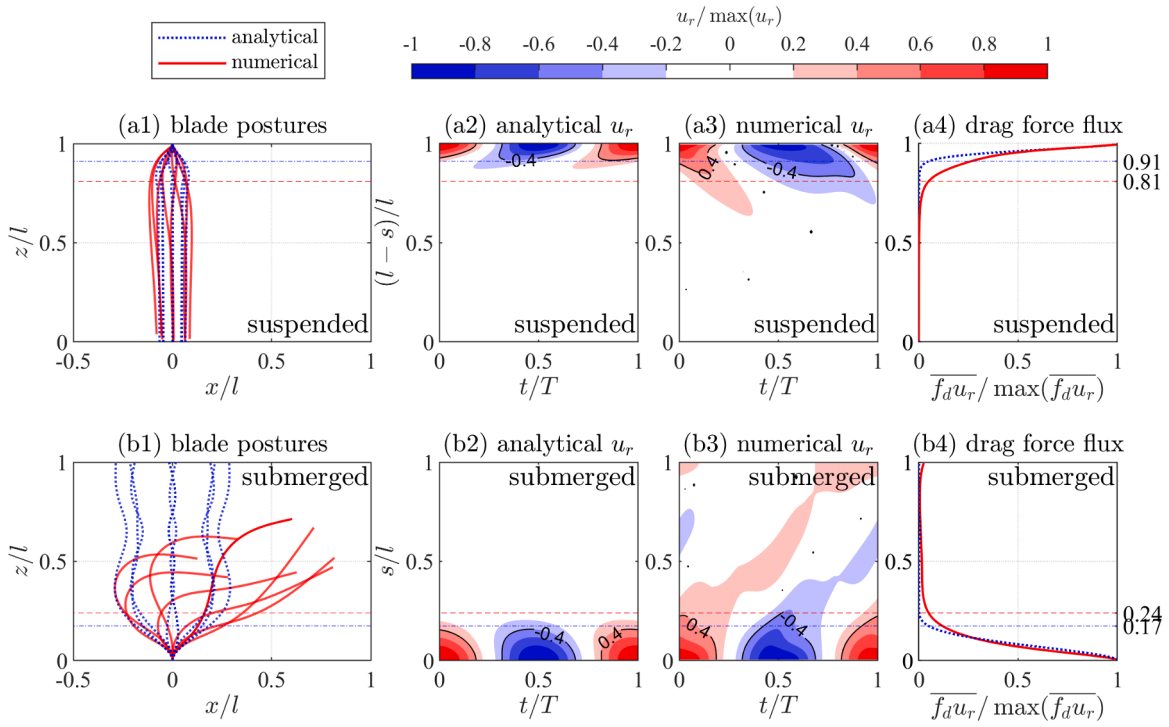

Fig. 9. Comparisons between the analytical (simplified linearized blade motion) and numerical (nonlinear blade motion) calculations for the (a1 and b1) blade postures (x, z), (a2, a3, b2, and b3) relative velocity (u_r), and (a4 and b4) time averaged drag flux ($\overline{f_d u_r}$) of the (a) suspended model kelp blade and (b) submerged model vegetation. The global coordinates (x, z) and local coordinate (s) are normalized by blade length (l). The time (t) is normalized by wave period (T). The horizontal lines indicate the vertical position where $\overline{f_d u_r} = 5\%\max(\overline{f_d u_r})$ with numerical calculations in red dashed lines and analytical calculations in blue dash dotted lines.

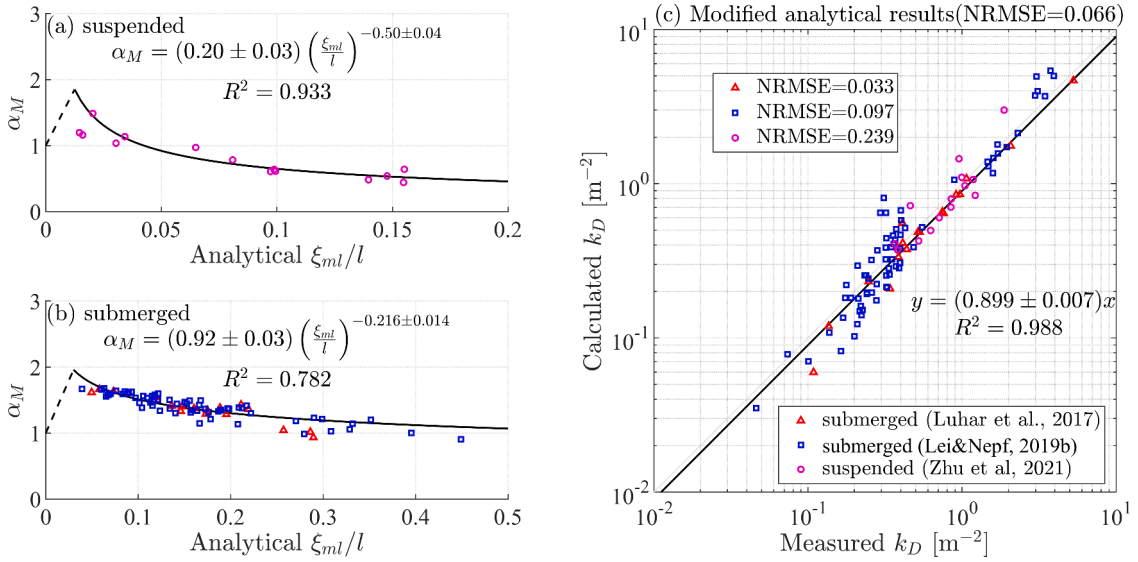

Fig. 10. The ratio of the wave decay coefficients by flexible blades calculated from the numerical model and that calculated from the analytical model (α_M) as a function of the blade motion amplitude at the blade tip normalized by the blade length (ξ_{ml}/l) for (a) suspended kelp and (b) submerged vegetation. The best fitting for the data is denoted by a black line with the formula and R^2 nearby. As the numerical results reduce to the analytical results for $\xi_{ml}/l \ll 1$, α_M approaches to 1 as ξ_{ml}/l approaches to 0. This (imaginary possible) trend out of the range of the data is denoted by dashed lines. (c) The wave decay coefficient (k_D) calculated from the modified analytical results using the ratio α_M compared with the measured k_D from Luhar et al. (2017) and Lei and Nepf (2019b) for submerged vegetation and Zhu et al. (2021) for suspended kelp. The normalized root mean square error (NRMSE) by the range of measured k_D is shown in the legend.

For the kelp, the designed length (l) of the kelp blade follows the measured data in Augyte et al. (2017) for the *Saccharina latissima* in Maine, USA (Fig. 11b). The corresponding blade width (b), maximum thickness (d_{max}), and elastic modulus (E) are calculated based on the relations with the blade length using the empirical formulas in Zhu et al. (2021) and shown in Fig. 11b. In Zhu et al. (2021), E was fitted as an exponential function of d_{max}, which may yield a very large E when d_{max} exceeds a critical value (e.g., $E > 100$ Pa if $d_{max} > 1.26$ mm). To avoid too large values for E, the maximum E is set as the measured maximum value 22 MPa in Zhu et al. (2021). This setting may underestimate the

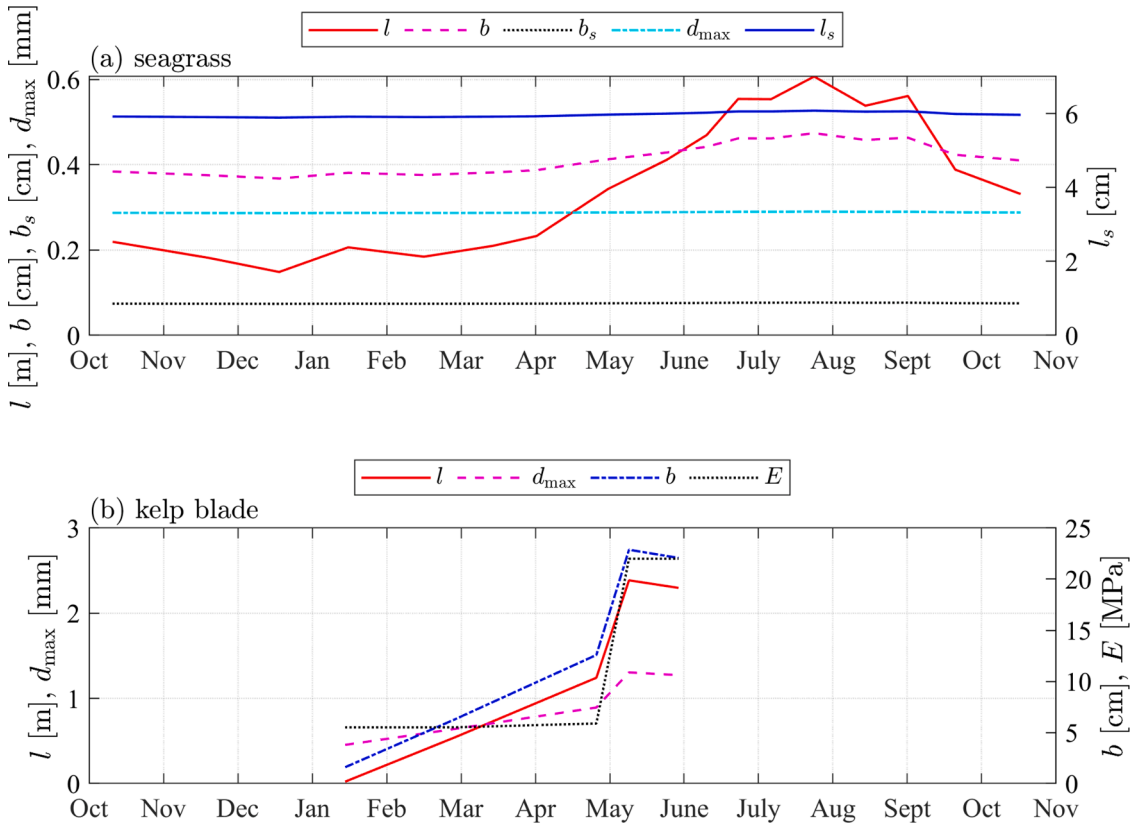

Fig. 11. The designed parameters for (a) seagrass and (b) kelp over one year. The parameters include blade length (l), blade width (b), blade maximum thickness ($d_{\max}$), and elastic modulus (E). The length and width for the seagrass sheath are l_s and b_s.

wave attenuation capacity of kelp in summer when the kelp blade is thick. It is noted that the blade thickness (d) decreases from the center of the blade width to both edges, following a normal-like distribution along the blade width (Zhu et al., 2021),

$$\frac{d}{d_{\max}} = (0.797 \pm 0.011)e^{-\frac{1}{2}\left(\frac{s_b/b}{0.118\pm0.003}\right)^2} + 0.203 \pm 0.011, \tag{34}$$

where s_b is the distance from the center of the blade width toward the blade edge. Based on the thickness distribution in (34), the second momentum of the cross section of *Saccharina latissima* is

$$I = \int_{-\frac{1}{2}d_{max}}^{\frac{1}{2}d_{max}} 2|s_b|y^2 dy \approx \frac{0.2bd_{max}^3}{12}, \tag{35}$$

indicating that the flexural rigidity of the real *Saccharina latissima* blade is only 20% of the same wide blade but with the maximum thickness. Therefore, an effective blade width with $b_e = 0.2b$ is used to calculate the flexural rigidity following Zhu et al. (2021). The designed mass density of kelp is 1053 kg/m^3, and the plant density is 405 plants/m (Zhu et al., 2021). The sheltering factor of $\alpha_e = 0.630$ (Zhu et al., 2021) is assumed to be applicable for this case study. Due to limited data for the stipes, the stipes were not considered in this study, which may underestimate the wave attenuation of the kelp farms. The kelp longline is designed at 1.2 m below the still water level and 4 m apart in 8 m-deep water. To compare with the seagrass meadow in the same water depth, a shallower water depth of 5 m is also considered for kelp farms. Since the kelp blade grows longer after May, the flexural rigidity decreases such that $|\gamma|$ can reach up to 1.67 in May, indicating a non-negligible role of buoyancy. Consequently, the neglecting of buoyancy might cause uncertainty in the wave attenuation.

For the wave conditions, the designed wave height is 1 m and the wave period is designed as 6 s. The drag coefficient C_d and added mass coefficient C_m are calculated using (9) and (10). The original analytical model without modification is used in this case study. To evaluate the wave attenuation performance of the canopies, the wave energy dissipation rate (EDR) is used and defined as

$$EDR = 1 - \frac{H(L_v)^2}{H(0)^2} = 1 - \left(\frac{1}{1 + k_D H_0 L_v}\right)^2, \tag{36}$$

where L_v is the canopy length in the direction of wave propagation. In this case study, the canopy length is designed as 200 m (50 longlines of kelp).

The wave attenuation by the designed suspended kelp farms and seagrass is shown in Fig. 12. The wave height decays when propagating through the canopy. The transmitted wave height varies seasonally, which is more obvious at the trailing edge of the canopy. To investigate the wave attenuation capacities of suspended kelp farms and seagrass, the EDRs at the trailing edge of the canopies are compared in Fig. 12d. The EDR shows a similar pattern to the variance of blade length around the year. The growth period of kelp has significant impacts on wave attenuation. Kelp is planted in late November after about 1.5 months of growth in a nursery and grows slowly over the first few months (Fig. 11b), resulting in a small EDR (<10%) during this time (Fig. 12d). After about five months of growth, the kelp blade length exceeds 1.5 m at the end of April, yielding considerable wave attenuation with EDR>10% in 8 m-deep water and EDR>20% in 5 m-deep water. When the kelp blade reaches 2.4 m long in May, the wave attenuations of kelp farms in 8-m deep water and 5 m-deep water are enhanced to 29% and 43%, respectively. The wave attenuation remains at this level until the kelp is harvested in June. Unlike the newly planted kelp with blades growing from millimeters to meters in the growing season, the averaged leaf length for a perennial seagrass meadow changes from 15 to 61 cm

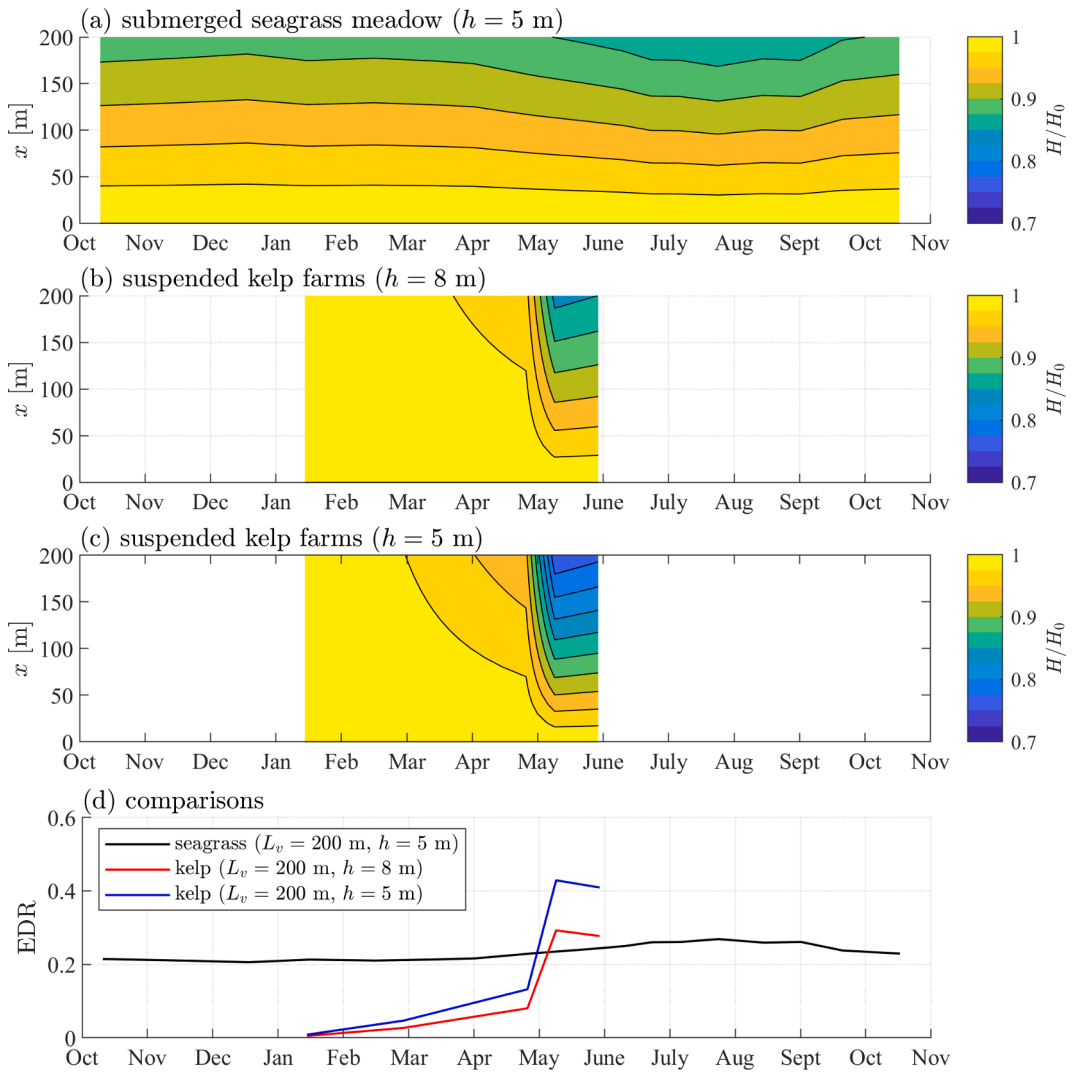

Fig. 12. Wave height decaying along the distance (x) in the canopies: (a) submerged seagrass meadow in 5 m-deep water (h), and suspended kelp farms in (b) 8 m-deep water and (c) 5 m-deep water. (d) Comparisons between the wave energy dissipation rate (EDR) by kelp and seagrass at the ending edge of the canopy. The canopy length (L_v) is 200 m. The designed wave height is 1 m and wave period is 6 s.

(Fig. 11a). Therefore, seagrass is less impacted by seasonal growth patterns that are typical of kelp farms. Compared to kelp farms, the seagrass has a larger elastic modulus and canopy density, yielding a larger EDR>20% than the kelp in the initial growing months with small blade lengths. However, the wave attenuation capacity of kelp farms surpasses the seagrass in the later months when the kelp blades become longer (>1.5 m). The EDR by seagrass is most significant at 27% in August when the leaf and sheath lengths are the longest.

4. Discussion

4.1. Evaluations and limitations of the analytical wave attenuation model

The analytical wave attenuation model performed well in predicting the wave attenuation of suspended and submerged canopies with a small NRMSE. Based on the analytical model, the analytical solutions for the bulk drag coefficient (C_D) and effective blade length (l_e) were obtained. Conventionally, C_D and l_e are usually fitted as a function of *KC* and *CaL*, respectively. The results showed that the analytically calculated C_D and l_e are in a similar precision to the *KC*-based fitting C_D and *CaL*-based fitting l_e. The *KC* describes the relative importance of drag force over inertia force on a rigid body, and the *CaL* scaling is developed based on the static balance of blade stiffness and drag force. The *KC*-based and *CaL*-based fitting did not incorporate all the parameters governing the wave-induced blade dynamics such as the frequency ratio, and therefore influence the precision of the fittings. However, due to the complicated wave-blade interaction, sophisticated parameters to obtain good fits (e.g., $R^2 > 0.8$) of C_D and l_e for a wide range of wave conditions and blade properties are difficult to achieve. Thus, the analytical solutions for C_D and l_e can be an alternative when reliable C_D and l_e are not available. Meanwhile, the analytical solutions for C_D and l_e have given the parameters that govern C_D and l_e, which may also provide insight into the appropriate parameters and relations to obtain a better fit for C_D and l_e. For example, the ratio of the blade's natural frequency and the wave frequency influences the resonance and therefore is an important parameter that should be incorporated into the development of the empirical formulas for C_D and l_e.

To obtain an explicit analytical solution for the wave attenuation, the blade dynamics are simplified and linearized by assuming negligible vertical forces (net buoyancy and friction) and a small-amplitude blade motion. However, the simplification and linearization decrease the precision for simulating the blade dynamics and the wave attenuation. To improve the model, a modification factor α_M can be used. In this study, the formulas (32) and (33) for α_M was fitted as a simple power function of the blade motion amplitude at the blade tip normalized by the blade length (ξ_{ml}/l) using limited data with $0.015 \leq \xi_{ml}/l \leq 0.155$

and $0.039 \leq \xi_{ml}/l \leq 0.449$ for suspended and submerged canopies, respectively. The flaw of this fitting is that the calculated α_M using (32) and (33) cannot converge to 1 as ξ_{ml}/l approaches to 0 when the numerical results reduce to the analytical results for rigid vegetation. Thus, the formulas (32) and (33) have limited application for the given range of ξ_{ml}/l. A more sophisticated fitting of α_M will be developed with more data in the future. Understanding the effects of neglecting buoyancy and the geometrical nonlinearity is helpful to improve the analytical solution.

The within canopy water velocity showed a phase lead and magnitude reduction relative to the above-canopy water velocity, especially for dense canopies Lowe et al., 2005; Rosman et al., 2013; Henderson et al., 2017). In this study, the magnitude reduction of the water velocity was considered using the approach in Lowe et al. (2005) while the phase shift was ignored. Supposing the phase shift is a constant or varies slowly in time and location, it is expected to have no effects on blade motion and wave attenuation because the phase shift is removed by time averaging in the model development. However, the phase shift changing with time and location may significantly affect blade dynamics and wave attenuation, which warrants further investigation. As waves propagate into the canopy interior, the wave height and wave orbital velocity decrease with distance into the canopy. Thus, the vegetation and kelp are under larger wave conditions at the leading edge of the canopy while under smaller wave conditions at the end of the canopy, resulting in different blade dynamics with distance along the canopy. The blade displacement is determined by the wave height H and transfer functions γ_s and $\gamma_c$as shown in ((14). To obtain the wave attenuation by solving the energy conservation Eq. (18), the blade displacement is treated using a decaying wave height $H(x)$ (because the wave height is the unknown) and distance-independent transfer functions γ_s and γ_c. Since the effects of wave height decay on blade dynamics were incorporated into the wave attenuation model, the effects induced by assuming distance-independent γ_s and γ_c are expected to be small in the prediction of wave attenuation. In this study, using the wave conditions at the leading edge and trailing edge of the canopy to estimate γ_s and γ_c was observed to have no difference on the prediction of the wave attenuation. This might be explained by the weak wave attenuation of flexible blades in the selected experiments with the minimum transmitted wave height as 75% of the incident wave height (the contribution of the rigid part of the blades was removed). For large wave attenuation, the error induced by assuming distance-independent γ_s and γ_c may appear, but it is still expected to be small in wave attenuation prediction because the wave height decay is considered.

The flexible vegetation and kelp blade have shown significant asymmetric motions. The asymmetry of the blade motion is induced by the vertical wave orbital velocity and the phase lag in encountering water velocity caused by blade displacement (Zhu et al., 2020b). This asymmetry occurs in linear waves and can be enhanced by wave nonlinearity. The mean blade tilt is large at the blade tip and decreases dramatically to the fixed end. Unfortunately, the analytical model cannot capture the asymmetric motion. However, as the blade segments near the tip with large mean tilt have very little contribution to the wave attenuation and only a few blade segments near the fixed end with small mean tilt dominate the wave attenuation, the effects of the large mean blade tilt may be small. Thus, the analytical model could perform well in predicting wave attenuation, although the asymmetric blade motion is not well predicted. Nevertheless, the effects of the mean blade tilt of the blade segments near the fixed end on wave attenuation might be significant and worth further study. The mean blade tilt might reduce the drag force and therefore reduce the wave attenuation. Thus, neglecting the mean blade tilt might overestimate the wave attenuation.

For a dense canopy, the blades are close to each other, yielding sheltering and interaction between blades. The sheltering effects can reduce the drag of the sheltered blades and therefore reduce the wave attenuation. For long kelp blades, blade interaction may result in the entanglement of the kelp blades, enhancing blade breakage (Koehl and Wainwright, 1977) and, therefore, influencing the wave attenuation. In this study, the kelp blade sheltering and interaction was considered using a constant factor, which should be improved by scaling with blade properties and configuration as well as wave conditions.

The analytical model was developed assuming monochromatic waves. In the real world, waves can be described using random waves with different frequencies. The form of the present analytical wave attenuation model for random waves is referred to Zhu et al. (2020a). However, for waves with strong nonlinearity and nonlinear wave-wave interaction, such as infragravity waves (Mullarney and Pilditch, 2017), the application of the present model warrants careful consideration. In the field, the background current also has significant influences on the reconfiguration of vegetation and kelp and waves (Gaylord et al., 2003; Rosman et al., 2003; Losada et al., 2016; Lei and Nepf, 2019a; Fredriksson et al., 2020; Zhang and Nepf, 2020, 2021; Lei et al., 2021), which should be also implemented in the future work.

4.2. Nature-based coastal protection strategies

The case study showed the wave attenuation capacity of *Saccharina latissima* varies seasonally with the kelp growth. After about 6.5 months of growth (1.5 months in the nursery and five months in the ocean), the kelp blade grows longer than 1.5 m and can provide considerable wave attenuation. For different locations (e.g., different water temperatures and salinities, different water depths, exposed sites, and sheltered sites, etc.), the growth rate may be different (Peteiro and Freire, 2013; Nielsen et al., 2014; Augyte et al., 2017; Vettori and Nikora,2017; Azevedo et al., 2019). Large wave conditions (with significant wave height greater than 1.5 m) associated with storm events typically occur in the Gulf of Maine, for example, in winter and spring from October to May (data from Maine EPSCoR SEANET Buoy C0502 in Saco Bay). To develop large kelp blades to provide considerable wave attenuation in winter, it is proposed that the kelp should be seeded several months earlier. As kelp grows faster in cold water, the kelp can be submerged near the seafloor during summer and then moved upward to the surface in winter. To keep considerable wave attenuation of kelp farms for coastal protection around the year, the biennial harvesting technique (Peteiro et al., 2006) could be adopted. As a result, the kelp older than one year can be several meters long, providing more favorable wave attenuation. One recommended strategy is to harvest every other longline every other year. To improve commercial values, the multiple partial harvesting technique (Bak et al., 2018) is also recommended such that only part of the blades is cut off, leaving an adequate length of the blade to allow regrowth and provide considerable wave attenuation. Since the kelp may get biofouled, degraded, and ragged in summer (Førde et al., 2016), one solution is to submerge the kelp canopy deep in water to improve the survivability (Peteiro et al., 2006). In addition to dissipating wave energy, kelp farms can also play a substantial role in marine carbon sequestration for climate change mitigation and adaptation (Krause-Jensen and Duarte, 2016; Duarte et al., 2017).

Unlike newly seeded kelp, naturally occurring seagrass is less impacted by seasonality. Implementing seagrass with kelp aquaculture may mitigate the seasonal impacts. In addition, combining seagrass and suspended kelp aquaculture structures can improve their wave attenuation capacity for a wider range of wave periods and water levels (Zhu et al., 2020a). Enhancing the size of kelp aquaculture farms and the plant density can also improve the wave attenuation capacity as expected (Zhu et al., 2021).

5. Conclusion

In this study, an analytical wave attenuation model for flexible vegetation and kelp was developed by simplifying and linearizing the blade motion. Compared with a wide range of experiments for submerged and suspended canopies with flexible blades, the simplified analytical model underestimated the wave decay coefficient by 27%, but

with a small NRMSE of 0.054. In comparison, the numerical model with full nonlinearity underestimated the wave decay coefficient by 11.7% with NRMSE = 0.063. To reduce the underestimation of the analytical model due to the simplification and linearization, a modification factor was developed, reducing the underestimation of the analytical model to 10.1%. Based on the analytical model, analytical solutions for the bulk drag coefficient (C_D) and effective blade length (l_e) were derived, which showed a similar precision with the experimentally fitted C_D and l_e, indicating that the analytical solutions for C_D and l_e could be a reliable alternative when the experimentally calibrated C_D and l_e are not available. The analytical solutions are computationally efficient and easy to implement into large-scale models to analyze the influences of wave attenuation on processes such as coastal morphology, inner shelf circulation, and material transport. A case study showed the wave attenuation of cultivated *Saccharina latissima* changes seasonally with the kelp growth. When the kelp blade reaches 2.4 m long after seven months of growth, the kelp farms with 50 longlines (over a distance of 200 m in the direction of wave propagation) in 8 m-deep water may attenuate wave energy by 29% for 1 m-high waves with the period of 6 s. The wave attenuation can be enhanced to 43% when the farms are located in 5 m-deep water. To provide considerable wave attenuation of kelp with adequate long blades around the year, biennial and multiple partial harvesting techniques are recommended. The research of using kelp aquaculture structures as nature-based coastal protection is still in its infancy. Field observations of wave attenuation by kelp aquaculture structure are an important research gap to consider for future studies.

CRediT authorship contribution statement

Longhuan Zhu: Conceptualization, Methodology, Software, Validation, Formal analysis, Investigation, Resources, Data curation, Writing – original draft, Writing – review & editing, Visualization. **Kimberly Huguenard:** Writing – review & editing, Supervision, Project administration. **David W. Fredriksson:** Writing – review & editing. **Jiarui Lei:** Conceptualization, Writing – review & editing.

Declaration of Competing Interest

The authors declare that they have no known competing financial interests or personal relationships that could have appeared to influence the work reported in this paper.

Acknowledgments

This work was completed as part of the PhD research of Longhuan Zhu who was supported by National Science Foundation award #IIA-1355457 to Maine EPSCoR at the University of Maine. The authors gratefully acknowledge the assistance of the Advanced Computing Group of the University of Maine System in producing the numerical data. Longhuan Zhu was benefited from the discussions with Gretchen Grebe and Zhilong Liu. Finally, the authors would like to thank the anonymous reviewers and associate editor for constructive comments that really helped to improve this manuscript greatly.

References

Abdelrhman, M., 2007. Modeling coupling between eelgrass Zostera marina and water flow. Mar. Ecol. Prog. Ser. 338, 81–96. https://doi.org/10.3354/meps338081.

Anderson, M.E., Smith, J.M., 2014. Wave attenuation by flexible, idealized salt marsh vegetation. Coastal Eng. 83, 82–92. https://doi.org/10.1016/j.coastaleng.2013.10.004.

Augyte, S., Yarish, C., Redmond, S., Kim, J.K., 2017. Cultivation of a morphologically distinct strain of the sugar kelp, Saccharina latissima forma angustissima, from coastal Maine, USA, with implications for ecosystem services. J. Appl. Phycol. 29 (4), 1967–1976. https://doi.org/10.1007/s10811-017-1102-x.

Azevedo, I.C., Duarte, P.M., Marinho, G.S., Neumann, F., Sousa-Pinto, I., 2019. Growth of Saccharina latissima (Laminariales, Phaeophyceae) cultivated offshore under exposed conditions. Phycologia 58 (5), 504–515. https://doi.org/10.1080/00318884.2019.1625610.

Bak, U.G., Mols-Mortensen, A., Gregersen, O., 2018. Production method and cost of commercial-scale offshore cultivation of kelp in the Faroe Islands using multiple partial harvesting. Algal Res. 33 (May), 36–47. https://doi.org/10.1016/j.algal.2018.05.001.

Borgman, L.E., 1967. Random hydrodynamic forces on objects. Ann. Math. Stat. 38 (1), 37–51. https://doi.org/10.1214/aoms/1177699057.

Bradley, K., Houser, C., 2009. Relative velocity of seagrass blades: implications for wave attenuation in low-energy environments. J. Geophys. Res. 114 (F1), F01004. https://doi.org/10.1029/2007JF000951.

Chen, H., Zou, Q.P., 2019. Eulerian–Lagrangian flow-vegetation interaction model using immersed boundary method and OpenFOAM. Adv. Water Resour. 126, 176–192. https://doi.org/10.1016/j.advwatres.2019.02.006.

Chen, H., Ni, Y., Li, Y., Liu, F., Ou, S., Su, M., Peng, Y., Hu, Z., Uijttewaal, W., Suzuki, T., 2018. Deriving vegetation drag coefficients in combined wave-current flows by calibration and direct measurement methods. Adv. Water Resour. 122, 217–227. https://doi.org/10.1016/j.advwatres.2018.10.008.

Chen, S.N., Sanford, L.P., Koch, E.W., Shi, F., North, E.W., 2007. A nearshore model to investigate the effects of seagrass bed geometry on wave attenuation and suspended sediment transport. Estuaries Coasts 30 (2), 296–310. https://doi.org/10.1007/BF02700172.

Currin, C.A., Chappell, W.S., Deaton, A., Shipman, H., Dethier, M.N., Gelfenbaum, G., Fresh, K.L., Dinicola, R.S., 2010. Developing alternative shoreline armoring strategies : the living shoreline approach in North Carolina. Shipman, Hugh and Dethier, Megan N. and Gelfenbaum, Guy and Fresh, Kurt L. and Dinicola, Richard S. (eds.). In: Puget Sound Shorelines and the Impacts of Armoring—Proceedings of a State of the Science Workshop. US Geological Survey, pp. 91–102. https://pubs.usgs.gov/sir/2010/5254/pdf/sir20105254_chap10.pdf.

Dalrymple, R.A., Kirby, J.T., Hwang, P.A., 1984. Wave diffraction due to areas of energy dissipation. J. Waterw. Port Coast. Ocean Eng. 110 (1), 67–79. https://doi.org/10.1061/(ASCE)0733-950X(1984)110:1(67).

Dean, R.G., Dalrymple, R.A., 1991. Water wave mechanics for engineers and scientists. Intergovernmental Panel on Climate Change. In: Advanced Series on Ocean Engineering, 2. World Scientific. https://doi.org/10.1142/1232.

Denny, M.W., Gaylord, B.P., Cowen, E.A., 1997. Flow and flexibility II. The roles of size and shape in determining wave forces on the bull kelp Nereocystis luetkeana. J. Exp. Biol. 200 (24), 3165–3183. https://jeb.biologists.org/content/200/24/3165.

Denny, M., Gaylord, B., 2002. The mechanics of wave-swept algae. J. Exp. Biol. 205 (Pt 10), 1355–1362. https://jeb.biologists.org/content/205/10/1355.short.

Denny, M., Gaylord, B., Helmuth, B., Daniel, T., 1998. The menace of momentum: dynamic forces on flexible organisms. Limnol. Oceanogr. 43 (5), 955–968. https://doi.org/10.4319/lo.1998.43.5.0955.

Duarte, C.M., Wu, J., Xiao, X., Bruhn, A., Krause-Jensen, D., 2017. Can seaweed farming play a role in climate change mitigation and adaptation? Front. Mar. Sci. 4 (APR), 100. https://doi.org/10.3389/fmars.2017.00100.

Elwany, M.H.S., O'Reilly, W.C., Guza, R.T., Flick, R.E, 1995. Effects of southern California Kelp beds on waves. J. Waterw. Port Coast. Ocean Eng. 121 (2), 143–150. https://doi.org/10.1061/(ASCE)0733-950X(1995)121:2(143).

Fonseca, M.S., Koehl, M.A.R., Kopp, B.S., 2007. Biomechanical factors contributing to self-organization in seagrass landscapes. J. Exp. Mar. Biol. Ecol. 340 (2), 227–246. https://doi.org/10.1016/j.jembe.2006.09.015.

Førde, H., Forbord, S., Handå, A., Fossberg, J., Arff, J., Johnsen, G., Reitan, K.I., 2016. Development of bryozoan fouling on cultivated kelp (Saccharina latissima) in Norway. J. Appl. Phycol. 28 (2), 1225–1234. https://doi.org/10.1007/s10811-015-0606-5.

Foster-Martinez, M.R., Lacy, J.R., Ferner, M.C., Variano, E.A., 2018. Wave attenuation across a tidal marsh in San Francisco Bay. Coast. Eng. 136, 26–40. https://doi.org/10.1016/j.coastaleng.2018.02.001.

Fredriksson, D.W., Dewhurst, T., Drach, A., Beaver, W., St. Gelais, A.T., Johndrow, K., Costa-Pierce, B.A, 2020. Hydrodynamic characteristics of a full-scale kelp model for aquaculture applications. Aquac. Eng. 90, 102086 https://doi.org/10.1016/j.aquaeng.2020.102086.

Fringer, O.B., Dawson, C.N., He, R., Ralston, D.K., Zhang, Y.J., 2019. The future of coastal and estuarine modeling: findings from a workshop. Ocean Model. 143, 101458 https://doi.org/10.1016/j.ocemod.2019.101458.

Gaeckle, J.L., Short, F.T., 2002. A plastochrone method for measuring leaf growth in eelgrass, Zostera marina L. Bull. Mar. Sci. 71 (3), 1237–1246. https://www.ingentaconnect.com/content/umrsmas/bullmar/2002/00000071/00000003/art00010.

Gaylord, B.P., Denny, M.W., Koehl, M.A.R., 2003. Modulation of wave forces on kelp canopies by alongshore currents. Limnol. Oceanogr. 48 (2), 860–871. https://doi.org/10.4319/lo.2003.48.2.0860.

Hansen, J.C.R., Reidenbach, M.A., 2013. Seasonal growth and senescence of a Zostera marina seagrass meadow alters wave-dominated flow and sediment suspension within a coastal bay. Estuaries Coasts 36 (6), 1099–1114. https://doi.org/10.1007/s12237-013-9620-5.

Henderson, S.M., 2019. Motion of buoyant, flexible aquatic vegetation under waves: simple theoretical models and parameterization of wave dissipation. Coast. Eng. 152, 103497 https://doi.org/10.1016/j.coastaleng.2019.04.009.

Henderson, S.M., Norris, B.K., Mullarney, J.C., Bryan, K.R., 2017. Wave-frequency flows within a near-bed vegetation canopy. Cont. Shelf Res. 147, 91–101. https://doi.org/10.1016/j.csr.2017.06.003.

Izaguirre, C., Méndez, F.J., Menéndez, M., Losada, I.J., 2011. Global extreme wave height variability based on satellite data. Geophys. Res. Lett. 38 (10) https://doi.org/10.1029/2011GL047302 n/a-n/a.

Jadhav, R.S., Chen, Q., Smith, J.M., 2013. Spectral distribution of wave energy dissipation by salt marsh vegetation. Coast. Eng. 77, 99–107. https://doi.org/10.1016/j.coastaleng.2013.02.013.

Keulegan, G.H., Carpenter, L.H., 1958. Forces on cylinders and plates in an oscillating fluid. J. Res. Natl. Bur. Stand 60 (5), 423–440 (1934). https://nvlpubs.nist.gov/nistpubs/jres/60/jresv60n5p423_A1b.pdf.
Kobayashi, N., Raichle, A.W., Asano, T., 1993. Wave attenuation by vegetation. J. Waterw. Port Coast. Ocean Eng. 119 (1), 30–48. https://doi.org/10.1061/(ASCE)0733-950X(1993)119:1(30).
Koch, E.W., Barbier, E.B., Silliman, B.R., Reed, D.J., Perillo, G.M.M.E., Hacker, S.D., Granek, E.F., Primavera, J.H., Muthiga, N., Polasky, S., Halpern, B.S., Kennedy, C.J., Kappel, C.V., Wolanski, E., 2009. Non-linearity in ecosystem services: temporal and spatial variability in coastal protection. Front. Ecol. Environ. 7 (Issue 1), 29–37. https://doi.org/10.1890/080126. Ecological Society of America.
Koehl, M.A.R., Wainwright, S.A., 1977. Mechanical adaptations of a giant kelp. Limnol. Oceanogr. 22 (6), 1067–1071. https://doi.org/10.4319/lo.1977.22.6.1067.
Krause-Jensen, D., Duarte, C.M., 2016. Substantial role of macroalgae in marine carbon sequestration. Nat. Geosci. 9 (10), 737–742. https://doi.org/10.1038/ngeo2790.
Lei, J., Fan, D., Angera, A., Liu, Y., Nepf, H., 2021. Drag force and reconfiguration of cultivated Saccharina latissima in current. Aquacult. Eng. 94, 102169 https://doi.org/10.1016/J.AQUAENG.2021.102169.
Lei, J., Nepf, H., 2019a. Blade dynamics in combined waves and current. J. Fluids Struct. 87, 137–149. https://doi.org/10.1016/j.jfluidstructs.2019.03.020.
Lei, J., Nepf, H., 2019b. Wave damping by flexible vegetation: connecting individual blade dynamics to the meadow scale. Coast. Eng. 147, 138–148. https://doi.org/10.1016/j.coastaleng.2019.01.008.
Losada, I.J., Maza, M., Lara, J.L., 2016. A new formulation for vegetation-induced damping under combined waves and currents. Coast. Eng. 107, 1–13. https://doi.org/10.1016/j.coastaleng.2015.09.011.
Lowe, R.J., 2005. Oscillatory flow through submerged canopies: 1. Velocity structure. J. Geophys. Res. 110 (C10), C10016. https://doi.org/10.1029/2004JC002788.
Luhar, M. 2012. Analytical and experimental studies of plant-flow interaction at multiple Scales. Doctoral dissertation, Massachusetts Institute of Technology. http://dspace.mit.edu/handle/1721.1/78142.
Luhar, M., Infantes, E., Nepf, H., 2017. Seagrass blade motion under waves and its impact on wave decay. J. Geophys. Res.: Oceans 122 (5), 3736–3752. https://doi.org/10.1002/2017JC012731.
Luhar, M., Nepf, H.M., 2016. Wave-induced dynamics of flexible blades. J. Fluids Struct. 61, 20–41. https://doi.org/10.1016/j.jfluidstructs.2015.11.007.
Marsooli, R., Orton, P.M., Mellor, G., 2017. Modeling wave attenuation by salt marshes in Jamaica Bay, New York, using a new rapid wave model. J. Geophys. Res. Oceans 122 (7), 5689–5707. https://doi.org/10.1002/2016JC012546.
Mattila, J., Chaplin, G., Eilers, M.R., Heck, K.L., O'Neal, J.P., Valentine, J.F, 1999. Spatial and diurnal distribution of invertebrate and fish fauna of a Zostera marina bed and nearby unvegetated sediments in Damariscotta River, Maine (USA). J. Sea Res. 41 (4), 321–332. https://doi.org/10.1016/S1385-1101(99)00006-4.
Mendez, F.J., Losada, I.J., 2004. An empirical model to estimate the propagation of random breaking and nonbreaking waves over vegetation fields. Coast. Eng. 51 (2), 103–118. https://doi.org/10.1016/j.coastaleng.2003.11.003.
Méndez, F.J., Losada, I.J., Losada, M.A., 1999. Hydrodynamics induced by wind waves in a vegetation field. J. Geophys. Res. 104 (C8), 18383–18396. https://doi.org/10.1029/1999JC900119.
Möller, I., 2006. Quantifying saltmarsh vegetation and its effect on wave height dissipation: results from a UK East coast saltmarsh. Estuar. Coast. Shelf Sci. 69 (3–4), 337–351. https://doi.org/10.1016/j.ecss.2006.05.003.
Möller, I., 2019. Applying uncertain science to nature-based coastal protection: lessons from shallow wetland-dominated shores. Front. Environ. Sci. 7 https://doi.org/10.3389/fenvs.2019.00049.
Möller, I., Spencer, T., 2002. Wave dissipation over macro-tidal saltmarshes: effects of marsh edge typology and vegetation change. J. Coast. Res. 36 (36), 506–521. https://doi.org/10.2112/1551-5036-36.sp1.506.
Morison, J.R., Johnson, J.W., Schaaf, S.A., 1950. The force exerted by surface waves on piles. J. Pet.Technol. 2 (05), 149–154. https://doi.org/10.2118/950149-G.
Mork, M., 1996. The effect of kelp in wave damping. Sarsia 80 (4), 323–327. https://doi.org/10.1080/00364827.1996.10413607.
Morris, R.L., Graham, T.D.J., Kelvin, J., Ghisalberti, M., Swearer, S.E., 2019. Kelp beds as coastal protection: wave attenuation of Ecklonia radiata in a shallow coastal bay. Ann. Bot. 125, 235–246. https://doi.org/10.1093/aob/mcz127.
Mullarney, J.C., Henderson, S.M., 2010. Wave-forced motion of submerged single-stem vegetation. J. Geophys. Res. 115 (C12), C12061. https://doi.org/10.1029/2010JC006448.
Mullarney, J.C., Pilditch, C.A., 2017. The differential response of kelp to swell and infragravity wave motion. Limnol. Oceanogr. 62 (6), 2524–2537. https://doi.org/10.1002/lno.10587.
Nielsen, M.M., Krause-Jensen, D., Olesen, B., Thinggaard, R., Christensen, P.B., Bruhn, A., 2014. Growth dynamics of Saccharina latissima (Laminariales, Phaeophyceae) in Aarhus Bay, Denmark, and along the species' distribution range. Mar. Biol. 161 (9), 2011–2022. https://doi.org/10.1007/s00227-014-2482-y.
Ondiviela, B., Losada, I.J., Lara, J.L., Maza, M., Galván, C., Bouma, T.J., van Belzen, J., 2014. The role of seagrasses in coastal protection in a changing climate. Coast. Eng. 87, 158–168. https://doi.org/10.1016/j.coastaleng.2013.11.005.
Ozeren, Y., Wren, D.G., Wu, W., 2014. Experimental investigation of wave attenuation through model and live vegetation. J. Waterw. Port Coast. Ocean Eng. 140 (5), 04014019 https://doi.org/10.1061/(ASCE)WW.1943-5460.0000251.
Pace, N.L., 2011. Wetlands or seawalls? Adapting shoreline regulation to address sea level rise and wetland preservation in the Gulf of Mexico. J. Land Use Environ. Law 26 (2), 327–363. https://www.jstor.org/stable/42842968.
Paul, M., Amos, C.L., 2011. Spatial and seasonal variation in wave attenuation over Zostera noltii. J. Geophys. Res. 116 (C8), C08019. https://doi.org/10.1029/2010JC006797.
Peteiro, C., Salinas, J., Freire, O., Fuertes, C., 2006. Cultivation of the autoctonus seaweed "Laminaria saccharina" off the Galician coast (NW Spain): production and features of the sporophytes for an annual and biennial harvest. Thalassas Int. J. Mar. Sci. 22 (1), 45–53. http://thalassas.webs.uvigo.es/Thalassas%2022(1)/T22(1)_5_Peteiro.pdf.
Peteiro, C., Freire, Ó., 2013. Biomass yield and morphological features of the seaweed Saccharina latissima cultivated at two different sites in a coastal bay in the Atlantic coast of Spain. J. Appl. Phycol. 25 (1), 205–213. https://doi.org/10.1007/s10811-012-9854-9.
Rao, S.S., 2007. Vibration of Continuous Systems. John Wiley & Sons, Inc. https://wp.kntu.ac.ir/hrahmanei/Adv-Vibrations-Books/Continuous-Vibrations-Rao.pdf.
Rosman, J.H., Denny, M.W., Zeller, R.B., Monismith, S.G., Koseff, J.R., 2013. Interaction of waves and currents with kelp forests (Macrocystis pyrifera): insights from a dynamically scaled laboratory model. Limnol. Oceanogr. 58 (3), 790–802. https://doi.org/10.4319/lo.2013.58.3.0790.
Sánchez-González, J.F., Sánchez-Rojas, V., Memos, C.D., 2011. Wave attenuation due to Posidonia oceanica meadows. J. Hydraul. Res. 49 (4), 503–514. https://doi.org/10.1080/00221686.2011.552464.
Sarpkaya, T., O'Keefe, J.L, 1996. Oscillating flow about two and three-dimensional bilge keels. J. Offshore Mech. Arct. Eng. 118 (1), 1–6. https://doi.org/10.1115/1.2828796.
Schulze, D., Rupprecht, F., Nolte, S., Jensen, K., 2019. Seasonal and spatial within-marsh differences of biophysical plant properties: implications for wave attenuation capacity of salt marshes. Aquat. Sci. 81, 65. https://doi.org/10.1007/s00027-019-0660-1.
Sollitt, C.K., Cross, R.H., 1972. Wave transmission through permeable breakwaters. Coast. Eng. Proc. 1 (13), 99. https://doi.org/10.9753/icce.v13.99.
Stevens, C.L., Hurd, C.L., Smith, M.J., 2001. Water motion relative to subtidal kelp fronds. Limnol. Oceanogr. 46 (3), 668–678. https://doi.org/10.4319/lo.2001.46.3.0668.
Sutton-Grier, A.E., Wowk, K., Bamford, H., 2015. Future of our coasts: the potential for natural and hybrid infrastructure to enhance the resilience of our coastal communities, economies and ecosystems. Environ. Sci. Policy 51, 137–148. https://doi.org/10.1016/j.envsci.2015.04.006.
Suzuki, T., Zijlema, M., Burger, B., Meijer, M.C., Narayan, S., 2012. Wave dissipation by vegetation with layer schematization in SWAN. Coast. Eng. 59 (1), 64–71. https://doi.org/10.1016/j.coastaleng.2011.07.006.
Syvitski, J.P.M., Kettner, A.J., Overeem, I., Hutton, E.W.H., Hannon, M.T., Brakenridge, G.R., Day, J., Vörösmarty, C., Saito, Y., Giosan, L., Nicholls, R.J., 2009. Sinking deltas due to human activities. Nat. Geosci. 2 (10), 681–686. https://doi.org/10.1038/ngeo629.
Tebaldi, C., Strauss, B.H., Zervas, C.E., 2012. Modelling sea level rise impacts on storm surges along US coasts. Environ. Res. Lett. 7 (1), 014032 https://doi.org/10.1088/1748-9326/7/1/014032.
Temmerman, S., Meire, P., Bouma, T.J., Herman, P.M.J., Ysebaert, T., De Vriend, H.J., 2013. Ecosystem-based coastal defence in the face of global change. Nature 504 (Issue 7478), 79–83. https://doi.org/10.1038/nature12859. Nature Publishing Group.
Utter, Denny, 1996. Wave-induced forces on the giant kelp Macrocystis pyrifera (Agardh): field test of a computational model. J. Exp. Biol. 199, 2645–2654. https://jeb.biologists.org/content/199/12/2645.short.
van Veelen, T.J., Fairchild, T.P., Reeve, D.E., Karunarathna, H., 2020. Experimental study on vegetation flexibility as control parameter for wave damping and velocity structure. Coast. Eng. 157, 103648 https://doi.org/10.1016/j.coastaleng.2020.103648.
Vettori, D., Nikora, V., 2017. Morphological and mechanical properties of blades of Saccharina latissima. Estuar. Coast. Shelf Sci. 196, 1–9. https://doi.org/10.1016/j.ecss.2017.06.033.
Vuik, V., Suh Heo, H.Y., Zhu, Z., Borsje, B.W., Jonkman, S.N., 2018. Stem breakage of salt marsh vegetation under wave forcing: a field and model study. Estuar Coast Shelf Sci 200, 41–58. https://doi.org/10.1016/j.ecss.2017.09.028.
Weinkle, J., Landsea, C., Collins, D., Musulin, R., Crompton, R.P., Klotzbach, P.J., Pielke, R., 2018. Normalized hurricane damage in the continental United States 1900–2017. Nature Sustainability 1 (12), 808–813. https://doi.org/10.1038/s41893-018-0165-2.
Zeller, R.B., Weitzman, J.S., Abbett, M.E., Zarama, F.J., Fringer, O.B., Koseff, J.R., 2014. Improved parameterization of seagrass blade dynamics and wave attenuation based on numerical and laboratory experiments. Limnol. Oceanogr. 59 (1), 251–266. https://doi.org/10.4319/lo.2014.59.1.0251.
Zhang, X., Nepf, H., 2020. Flow-induced reconfiguration of aquatic plants, including the impact of leaf sheltering. Limnol. Oceanogr. 65 (11), 2697–2712. https://doi.org/10.1002/lno.11542.
Zhang, X., Nepf, H., 2021. Wave damping by flexible marsh plants influenced by current. Phys. Rev. Fluids 6 (10), 1–17. https://doi.org/10.1103/physrevfluids.6.100502.
Zhu, L., Chen, Q., 2015. Numerical modeling of surface waves over submerged flexible vegetation. J. Eng. Mech. 141 (8), A4015001 https://doi.org/10.1061/(ASCE)EM.1943-7889.0000913.
Zhu, L., 2020. Wave Attenuation Capacity of Suspended Aquaculture Structures with Sugar Kelp and Mussels. Doctoral dissertation. University of Maine. http://digitalcommons.library.umaine.edu/etd/3222/" xlink:role="http://www.elsevier.com/xml/linking-roles/preprint">http://digitalcommons.library.umaine.edu/etd/3222/.

Zhu, L., Huguenard, K., Fredriksson, D., 2018. Interaction between waves and hanging highly flexible kelp blades. Coast. Eng. Proc. 1 (36), 31. https://doi.org/10.9753/icce.v36.papers.31.

Zhu, L., Huguenard, K., Zou, Q., Fredriksson, D.W., Xie, D., 2020a. Aquaculture farms as nature-based coastal protection: random wave attenuation by suspended and submerged canopies. Coast. Eng. 160, 103737 https://doi.org/10.1016/j.coastaleng.2020.103737.

Zhu, L., Lei, J., Huguenard, K., Fredriksson, D.W., 2021. Wave attenuation by suspended canopies with cultivated kelp (Saccharina latissima). Coast. Eng., 103947 https://doi.org/10.1016/j.coastaleng.2021.103947.

Zhu, L., Zou, Q., 2017. Three-layer analytical solution for wave attenuation by suspended and nonsuspended vegetation canopy. Coast. Eng. Proc. 1 (35), 27. https://doi.org/10.9753/icce.v35.waves.27.

Zhu, L., Zou, Q., Huguenard, K., Fredriksson, D.W., 2020b. Mechanisms for the asymmetric motion of submerged aquatic vegetation in waves: a consistent-mass cable model. J. Geophys. Res.: Oceans 125 (2), 1–31. https://doi.org/10.1029/2019JC015517.